A Mathematical Model of Solute Coupled Water Transport in Toad Intestine Incorporating Recirculation of the Actively Transported Solute

Erik Hviid Larsen,* Jakob Balslev Sørensen,* and Jens Nørkær Sørensen‡

From the From the *Zoophysiological Laboratory, August Krogh Institute, The University of Copenhagen, DK-2100 Copenhagen Ø; and ‡Department of Fluid Mechanics, Building 403, Technical University of Denmark, DK-2800 Lyngby, Denmark

abstract A mathematical model of an absorbing leaky epithelium is developed for analysis of solute coupled water transport. The non-charged driving solute diffuses into cells and is pumped from cells into the lateral intercellular space (*lis*). All membranes contain water channels with the solute passing those of tight junction and interspace basement membrane by convection-diffusion. With solute permeability of paracellular pathway large relative to paracellular water flow, the paracellular flux ratio of the solute (influx/outflux) is small (2–4) in agreement with experiments. The virtual solute concentration of fluid emerging from *lis* is then significantly larger than the concentration in *lis*. Thus, in absence of external driving forces the model generates isotonic transport provided a component of the solute flux emerging downstream *lis* is taken up by cells through the serosal membrane and pumped back into *lis*, i.e., the solute would have to be recirculated. With input variables from toad intestine (Nedergaard, S., E.H. Larsen, and H.H. Ussing, *J. Membr. Biol.* 168:241–251), computations predict that 60–80% of the pumped flux stems from serosal bath in agreement with the experimental estimate of the recirculation flux. Robust solutions are obtained with realistic concentrations and pressures of *lis*, and with the following features. Rate of fluid absorption is governed by the solute permeability of mucosal membrane. Maximum fluid flow is governed by density of pumps on *lis*-membranes. Energetic efficiency increases with hydraulic conductance of the pathway carrying water from mucosal solution into *lis*. Uphill water transport is accomplished, but with high hydraulic conductance of cell membranes strength of transport is obscured by water flow through cells. Anomalous solvent drag occurs when back flux of water through cells exceeds inward water flux between cells. Molecules moving along the paracellular pathway are driven by a translateral flow of water, i.e., the model generates pseudo-solvent drag. The associated flux-ratio equation is derived.

key words: isotonic transport • convection-diffusion • uphill water transport • anomalous solvent drag • pseudo-solvent drag

INTRODUCTION

Water transport by leaky vertebrate epithelia like small intestine (Curran and Solomon, 1957), gallbladder (Diamond, 1964a,b), and kidney proximal tubule (Windhager et al., 1958), which can occur in absence of external driving force, is coupled to active Na^+ transport. Since the first theoretical papers by Curran and MacIntosh (1962) and Patlak et al. (1963) a growing physiological literature has been concerned with analysis of physical mechanisms by which metabolic energy spend by a solute pump can be used for transporting solutes and water in isotonic or near-isotonic proportions through an epithelium (reviewed in Weinstein, 1994). The present paper contains such an analysis based on the concept that an actively transported solute, which is pumped into the lateral intercellular space, is recirculated via cells (Ussing and Eskesen, 1989; Ussing and Nedergaard, 1993; Ussing et al., 1996). The mathematical model contains dimensionless, well-stirred compartments, compliant plasma membranes, a non-electrolyte as driving species, and is solved for stationary states, only. Input parameters of the model are derived from a recent experimental study of toad small intestine providing cellular and paracellular unidirectional Na^+ fluxes and the first quantitative estimate of Na^+ recirculation in an absorbing epithelium (Nedergaard et al., 1999). After a discussion of physical properties of the paracellular pathway that have to be fulfilled for reproducing measured solute flux-ratio, the robustness of mathematical solutions is analyzed. We present computations aiming at investigating how well the framework predicts features of leaky vertebrate epithelia in general. Specifically, we analyze osmotic concentration and hydrostatic pressure of the lateral intercellular space, relationship between net solute flow and metabolic energy consumption, dependence of net water flux on density of solute pumps, paracellular convection, uphill water transport, and anomalous and pseudo-solvent drag. Computations based on this model have been presented as a brief report (Larsen and Sørensen, 1999).

Description of the Recirculation Model

The model contains three different pore types in cellular, tight-junction and interspace basement mem-

Address correspondence to Erik Hviid Larsen, August Krogh Institute, Universitetsparken 13, DK-2100 Copenhagen Ø, Denmark. Fax: 45-3532-1567; E-mail: EHLarsen@aki.ku.dk

branes: A diffusion pore (channel) is a water impermeable, but solute permeable pore, a convection-diffusion pore is a water and solute permeable pore, and a water pore (channel) is a water permeable, but solute impermeable pore (i.e., a pore with reflection coefficient of unity for the solute).

METHODS

Compartments and Membrane Pathways

The physical outline of the model is shown in Fig. 1, and the name and definition of the associated variables are listed in the Abbreviations. The outer and inner border of the epithelium are exposed to a mucosal (*o*)[1] and a serosal (*i*) compartment that are well stirred. The cellular (*cell*) and lateral intercellular space (*lis*) constitute two well-stirred intraepithelial compartments. The model contains the following five membranes, apical cell membrane (*a*), serosal cell membrane (*s*), lateral cell membrane (*lm*), tight junction membrane (*tm*), and interspace basement membrane (*bm*). The following solutes (all non-electrolytes) are considered: A diffusible solute, *S*, and non-diffusible solutes, *ND*, of the cellular and of the two external compartments. The diffusible solute, *S*, is supposed to pass all membranes, but by various mechanisms. An active, saturating pump is located in the membrane lining the lateral intercellular space. The tight junction and the interspace basement membrane contain both pure diffusion channels and convection-diffusion channels through which *S* is translocated by both convection and diffusion. Only in these membranes is water interacting with solute. The three other membranes contain water channels, and the serosal and apical membrane diffusion channels. By having both convection-diffusion and pure diffusion channels in tight junction membrane, paracellular convection fluxes can be analyzed for the case of convection-diffusion and pure diffusion, respectively, across tight junction.

Equations

In this section are presented the equations, which constitute the mathematical problem. There are four diffusion fluxes given by Fick's Law:

$$J_S^g = P_S^g(C_S^g - C_S^{cell}) \tag{1}$$

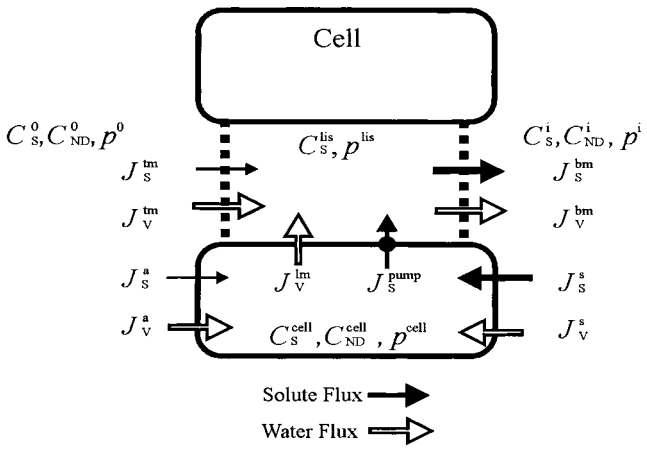

Figure 1. Recirculation model of solute coupled fluid transport in leaky absorbing epithelium. Parameters of the model are defined in the abbreviations. Fluxes of diffusible solute, J_S^m, and water, J_V^m, are given with reference to membrane, with $m = a$ indicating apical, $m =$ s indicating serosal, and $m = lm$ indicating lateral cell membrane, and *tm* and *bm* being the tight junction and interspace basement membrane, respectively. C_S^{comp} and C_{ND}^{comp} are concentrations of diffusible and non-diffusible solute, respectively, with compartment, *comp*, being either, $o =$ outer bath, *cell* = epithelial cell water, *lis* = lateral intercellular space, or $i =$ inner bath. p^{comp} indicates hydrostatic pressure of the compartment. Arrows associated with fluxes show direction of flows under physiological conditions. (Bottom) Flows from left to right, and from cell to lateral intercellular space, are considered positive. Above symbols and conventions are used in remaining figures.

$$J_S^s = P_S^s(C_S^{cell} - C_S^i) \tag{2}$$

$$J_S^{tm,\,diff} = P_S^{tm,\,diff}(C_S^g - C_S^{lis}) \tag{3}$$

$$J_S^{bm,\,diff} = P_S^{bm,\,diff}(C_S^{lis} - C_S^i) \tag{4}$$

The pump flux of the driving species is given by:

$$J_S^{pump} = P_S^{max,\,pump}\left(\frac{C_S^{cell}}{K_S^{pump} + C_S^{cell}}\right)^n \tag{5}$$

In all computations, $n = 3$ and $K_S^{pump} = 10$ mM.

In our treatment of coupling between solute and water flows in convection-diffusion channels we have avoided linearized forms of the Kedem-Katchalsky equation (Kedem and Katchalsky, 1958), which would make it necessary to deal with an average solute concentration in the pore. Instead we follow the suggestion by Patlak et al. (1963) by applying the differential equation (stationary conditions are assumed):

$$J_S = -D\frac{dC}{dx} + J_V(1-\sigma)C \tag{6}$$

where J_S is the solute flux, J_V the water-volume flux, C the solute concentration, and σ the reflection coefficient; $J_V(1-\sigma)$ is the convection velocity of the solute. This equation follows from the Smoluchowski equation (Smoluchowski, 1915) under stationary conditions (Sten-Knudsen, 1978) or from the Kedem-Kachalsky equation (Patlak et al., 1963). This type of problem was first dealt with by Hertz (1922). When integrated across the membrane the

[1] *Abbreviations used in this paper:* (Superscripts: compartments, membranes, and pathways) *a*, apical cell membrane; *bm*, interspace basement membrane; *c*, cell; *i*, inside (serosal) bath; *lis*, lateral intercellular space; *lm*, lateral cell membrane lining *lis*; *o*, outside (mucosal) bath; *s*, serosal cell membrane; *tm*, tight junction membrane; α, compartment (α = *o*, *c*, *lis*, or *i*); *m*, membrane (*m* = *a*, *s*, *lm*, *tm*, or *bm*); (Subscripts: solutes, water) *ND*, non-diffusible solute (cell or bath); *S*, driving (diffusible) solute; *T*, paracellular tracer; *V*, volume (water); (Intensive variables) C_S^α, concentration of *S* in α mM; C_{ND}^α, concentration of *ND* in α mM; *TON*, concentration of net transportate mM; D^{cell}, cell density; M_{ND}^{cell}, amount of ND per cell; V^{cell}, cell volume; p^α, hydrostatic pressure of α; (Membrane parameters) P_S^m, permeability to *S* in *m*; $P_S^{m,\,diff}$, permeability to *S* of pure diffusion pore in *tm* or *bm*; *n*, binding sites of pump dimensionless; L^m, hydraulic permeability of *m*; $\frac{\mu^m}{\mu^{cell}}$, relative compliance constant of *m* dimensionless; σ^m, reflection coefficient to *S* of convection-diffusion pore *tm* or *bm* dimensionless; (fluxes) J_S^m, flux of *S* across *m*; J_S^{pump}, pumped flux of *S* across *lm*; $J_S^{pump,\,max}$, saturated pump flux across *lm*; $J_S^{m,\,diff}$, flux of *S* in pure diffusion pore of *tm* or *bm*; $J_S^{para,\,IN}$, paracellular unidirectional influx of *S*; $J_S^{para,\,OUT}$, paracellular unidirectional outflux of *S*; J_V^m, water flux across *m*; J_V, transepithelial water flux.

resulting solution for J_s becomes[2] (denoted the Hertz equation):

$$J_S^{tm} = J_V^{tm}(1-\sigma^{tm})\frac{C_S^o \exp(J_V^{tm}(1-\sigma^{tm})/P_S^{tm}) - C_S^{lis}}{\exp(J_V^{tm}(1-\sigma^{tm})/P_S^{tm}) - 1} \quad (7)$$

$$J_S^{bm} = J_V^{bm}(1-\sigma^{bm})\frac{C_S^{lis} \exp(J_V^{bm}(1-\sigma^{bm})/P_S^{bm}) - C_S^{i}}{\exp(J_V^{bm}(1-\sigma^{bm})/P_S^{bm}) - 1} \quad (8)$$

The water flux through the five membranes are calculated from:

$$J_V^a = L^a\{RT(C_S^{Cell} + C_{ND}^{Cell} - C_S^o - C_{ND}^o) + (p^o - p^{cell})\} \quad (9)$$

$$J_V^s = L^s\{RT(C_S^i + C_{ND}^i - C_S^{Cell} - C_{ND}^{Cell}) + (p^{cell} - p^i)\} \quad (10)$$

$$J_V^{lm} = L^{lm}\{RT(C_S^{lis} - C_S^{Cell} - C_{ND}^{Cell}) + (p^{cell} - p^{lis})\} \quad (11)$$

$$J_V^{tm} = L^{tm}\{RT[\sigma^{tm}(C_S^{lis} - C_S^o) - C_{ND}^o] + (p^o - p^{lis})\} \quad (12)$$

$$J_V^{bm} = L^{bm}\{RT[\sigma^{bm}(C_S^i - C_S^{lis}) + C_{ND}^i] + (p^{lis} - p^i)\} \quad (13)$$

It follows that water channels of membranes *a, s,* and *lm* are not permeable to the solute, i.e., formally, σ^a, σ^s, and σ^{lm} are all unity. Requirement of mass conservation of diffusible solute and water, respectively, result in four continuity equations:

$$J_S^a = J_S^{ump} + J_S^s \quad (14)$$

$$J_S^{tm} = J_S^{tm} + J_S^{ump} + J_S^{tm,diff} - J_S^{bm,diff} \quad (15)$$

$$J_V^a = J_V^s + J_V^{lm} \quad (16)$$

$$J_V^{bm} = J_V^{tm} + J_V^{lm} \quad (17)$$

Inserting Eqs. 1–5 and 7–13 into the conservation equations results in four equations for the pressures and concentrations in the two intraepithelial compartments. In fact, the fluxes given by Eqs. 1– 5 and 7–13 are to be considered as auxiliary variables defining the various mechanisms by which solute transport takes place between compartments. The primary variables are the concentration of diffusible solutes, C_S^{cell} and C_S^{lis}, that are conserved through Eqs. 14 and 15, and the pressures, p^{cell} and p^{lis}, that serve to ensure mass conservation through Eqs. 16 and 17. It is important to note that the concentration of non-diffusible solute, C_{ND}^{cell}, only indirectly contributes to the conservation equations since it is not actively involved in the flux balance. As a consequence, the resulting system of equations contains five unknowns but only four equations. However, introducing an auxiliary pressure variable,

$$p^{*,cell} = p^{cell} - R \cdot T \cdot C_{ND}^{cell} \quad (18)$$

results in a unique system consisting of four equations to be solved for the four dependent variables, C_S^{cell}, C_S^{lis}, p^{lis}, and $p^{*,cell}$. Although the actual values of p^{cell} and C_{ND}^{cell} are not needed for the mathematical solution of the problem, they are of interest for discussing the physical processes involved. An additional equation for determining these variables can be established if the cell volume is known. The cell volume per unit area of epithelium, V^{cell}, is related to C_{ND}^{cell} from the equation,

$$V^{cell} \cdot C_{ND}^{cell} = D^{cell} \cdot M_{ND}^{cell} \quad (19)$$

in which the independent variables, D^{cell} and M_{ND}^{cell}, are the number of cells per unit area of epithelium and the amount of non-diffusible solute per cell, respectively. If the cell was rigid both V^{cell} and C_{ND}^{cell} would be constants, independent of the properties of mucosal and serosal bathing media. As discussed in Weinstein and Stephenson (1981) it is reasonable to incorporate a compliance model that takes into account pressure differences across compliant plasma membranes. Assuming a linear relationship between cell volume and cell pressure we can write,

$$\frac{V^{cell} - \hat{V}^{cell}}{\hat{V}^{cell}} = \mu^a \cdot (p^{cell} - p^o) + \mu^s \cdot (p^{cell} - p^i) + \mu^{lm} \cdot (p^{cell} - p^{lis}) \quad (20a)$$

Here, μ^a, μ^s, and μ^{lm} are compliance constants (Pa^{-1}) of the respective plasma membrane domains and $\hat{V}^{cell}$ the cell volume at pressure equilibrium between all compartments. Thus, knowing the cell volume at pressure equilibrium would in principle allow us to determine p^{cell}, C_{ND}^{cell}, and V^{cell} by solving Eqs. 18–20a. Unfortunately, neither compliance constants nor equilibrium conditions are known and we abstain from estimating these. It should be stressed, however, that with the introduction of the auxiliary variable, $p^{*,cell}$, Eqs. 1–5 and 7–18, constitute a unique system, which does not depend on any of these quantities, and which can be solved for all remaining dependent variables. An approximate way to proceed is to assume that the relative change in cell volume is so small that it can be neglected. This would imply that the cell volume displaced by, e.g., a pressure induced expansion of the lateral space, by the associated increasing p^{cell} causes a quantitative similar displacement of volume of the infinitely large external compartments. With this assumption Eq. 20a leads to,

$$p^{cell} = \frac{\mu^a}{\mu^{cell}} \cdot p^o + \frac{\mu^s}{\mu^{cell}} \cdot p^{lis} + \frac{\mu^{lm}}{\mu^{cell}} \cdot p^i \quad (20b)$$

where $\mu^{cell} = \mu^a + \mu^{lm} + \mu^s$. Thus, according to this model the hydrostatic pressure of the cell, p^{cell}, adjusts itself to a value between the ambient pressures weighted relative to local compliance constants. With $p^{*,cell}$ being obtained together with the other primary variables, C_S^{cell}, C_S^{lis}, p^{lis}, and the fluxes, as explained below (Computing Strategy), subsequently the three remaining unknowns, p^{cell}, C_{ND}^{cell}, and V^{cell}, are computed from Eqs. 18, 19, and 20b.

Paracellular unidirectional fluxes. The model contains equations for handling unidirectional paracellular fluxes of the driving species, *S*, as well as of solute(s) that cannot pass the cell (paracellular tracers, *T*). Unidirectional convection-diffusion fluxes of *S* across the tight junction membrane and the interspace basement membrane, respectively, are given by (always positive):

$$J_S^{tm,IN} = J_V^{tm}(1-\sigma^{tm})\frac{C_S^o \exp(J_V^{tm}(1-\sigma^{tm})/P_S^{tm})}{\exp(J_V^{tm}(1-\sigma^{tm}/P_S^{tm}) - 1)} \quad (21a)$$

$$J_S^{tm,OUT} = J_V^{tm}(1-\sigma^{tm})\frac{C_S^{lis}}{\exp(J_V^{tm}(1-\sigma^{tm}/P_S^{tm}) - 1)} \quad (21b)$$

$$J_S^{bm,IN} = J_V^{bm}(1-\sigma^{bm})\frac{C_S^{lis} \exp(J_V^{bm}(1-\sigma^{bm})/P_S^{bm})}{\exp(J_V^{bm}(1-\sigma^{bm}/P_S^{bm}) - 1)} \quad (22a)$$

$$J_S^{bm,OUT} = J_V^{bm}(1-\sigma^{bm})\frac{C_S^{i}}{\exp(J_V^{bm}(1-\sigma^{bm}/P_S^{bm}) - 1)} \quad (22b)$$

Equations for calculating unidirectional fluxes of *S* in diffusion channels of the interspace-membranes are:

[2]The assumptions underlying this equation are listed by Patlak et al. (1963). Most significantly, the partition coefficient is unity.

$$J_S^{tm,\,diff,\,IN} = P_S^{tm,\,diff} C_S^g \tag{23a}$$

$$J_S^{tm,\,diff,\,OUT} = P_S^{tm,\,diff} C_S^{lis} \tag{23b}$$

$$J_S^{bm,\,diff,\,IN} = P_S^{bm,\,diff} C_S^{lis} \tag{24a}$$

$$J_S^{bm,\,diff,\,OUT} = P_S^{bm,\,diff} C_S^{i} \tag{24b}$$

From the above fluxes, the two paracellular unidirectional fluxes of *S*, denoted $J_S^{para,\,IN}$ and $J_S^{para,\,OUT}$, respectively, are calculated by:

$$J_S^{para,\,IN} = \left(J_S^{tm,\,IN} + J_S^{tm,\,diff,\,IN}\right) \cdot \frac{J_S^{bm,\,IN} + J_S^{bm,\,diff,\,IN}}{J_S^{tm,\,OUT} + J_S^{tm,\,diff,\,OUT} + J_S^{bm,\,IN} + J_S^{bm,\,diff,\,IN}} \tag{25a}$$

$$J_S^{para,\,OUT} = \left(J_S^{bm,\,OUT} + J_S^{bm,\,diff,\,OUT}\right) \cdot \frac{J_S^{tm,\,OUT} + J_S^{tm,\,diff,\,OUT}}{J_S^{bm,\,IN} + J_S^{bm,\,diff,\,IN} + J_S^{tm,\,OUT} + J_S^{tm,\,diff,\,OUT}} \tag{25b}$$

These equations cover the case of steady state unidirectional fluxes of a three-compartment two-barrier system (Ussing and Zerahn, 1951). As an example, Eq. 25a can be taken to express that the probability of a molecule entering the sub-compartment from the mucosal solution via the *tm*-pathways proceeds to the serosal bath via the *bm*-pathways, is given by the ratio of fluxes through the *bm*-pathways and the sum of fluxes out of the sub-compartment. These equations are used also for calculating fluxes of the paracellular marker molecules, *T*, that do not permeate plasma membranes. Eqs. 25a and 25b are general for two parallel pathways in tight junction and interspace basement membrane, respectively. In the computations we deal with two cases, (a) the paracellular flux of *S* (and *T*) is governed by convection-diffusion in both membranes, and (b) the paracellular flux of *S* (and *T*) is governed by pure diffusion across the tight junction membrane and convection-diffusion across the basement membrane. Calculation of paracellular fluxes are performed after the mathematical solution defined by a given set of independent variables has been found.

Sign conventions. Fluxes of solute and water are positive in direction from outer to inner solution and from cell to lateral intercellular space.

Computing Strategy

We built two versions of the model: Solution of Eqs. 1–5, 7–17, 19, 20, and 25a,b) yields the value of the 20 dependent variables, but allows the net tonicity, *TON*, of the absorbed fluid to be a derived dependent variable:

$$TON = \frac{J_S^{bm} + J_S^{bm,\,diff} + J_S^{\S}}{J_V^{bm} + J_V^{s}} \tag{26}$$

Thus, in this version of the model (version 1), dependent on choices of independent variables, the net tonicity may vary from hypotonic over isotonic to hypertonic. To study the model under conditions of strictly isotonic transport, in the other version of the model (version 2), *TON*, was included as an independent variable, and Eqs. 2 and 26 were used for deriving an expression for $P_S^{\S}$:

$$P_S^{\S} = \frac{TON \cdot (J_V^{bm} + J_V^{s}) - J_S^{bm} - J_S^{tm,\,diff}}{C_S^{cell} - C_S^{i}} \tag{27}$$

In version 2 of the model, therefore, with *TON* set to isotonicity (300 mM), $P_S^{\S}$ was included as a dependent variable, defining the recirculation flux across the basolateral membrane that would make the net absorbate truly isotonic. The physiological implication of this procedure would seem to be that the epithelium actively regulates the recirculation pathway to achieve isotonicity. While this is a reasonable or at least a possible hypothesis, it is not a necessary implication of the mathematical procedure. Since in this paper we wish to study isotonic transport, the condition of isotonicity has to be included in the set of equations to assure that the identified mathematical solutions are in the isotonic area of parameter space. For the computations, we have chosen to make $P_S^{\S}$ a dependent variable. This, however, is only of historical interest once relevant mathematical solutions (reference states) have been identified. In real life it may as well be another parameter (for instance P_S^g) or a combination of two or more parameters, which is/are being regulated. Nevertheless, when isotonicity is assumed (version 2) it is important to remember that changing one parameter (see Figs. 4–8) is going to affect the values of all the derived variables (including $P_S^{\S}$).

Eqs. 1–5, 7–18, and 27 constitute a set of strongly coupled, non-linear equations for 17 (version 1) or 18 (version 2) dependent variables, respectively. A convenient way of solving this system is to use the iterative Newton-Raphson method, which is a computationally efficient and robust method for non-linear equations. With this method linearization is introduced locally by forming the Jacobian matrix by differentiating the governing equations with respect to the dependent variables.

Presentation of Results

All variables of the computer program are in SI units. For making comparison with experimental results from literature easy, as listed in the Abbreviations above, computed results given in the main text are in units common to physiological papers. However, in the physiological literature hydraulic conductance can be found in many different units. In tables and figures of the present paper is the hydraulic conductance of membrane *m*, L^m, given in units of $(cm \cdot s^{-1})/(N \cdot cm^{-2})$, which is related to the osmotic permeability, P_f, by:

$$P_f = \frac{R \cdot T \cdot L^m}{V_W} \tag{28a}$$

With the molar volume of water, $V_W = 18$ cm^3/mole, $R = 8.31(N \cdot 10^2\ cm) \cdot mole^{-1} \cdot K^{-1}$ and $T = 293$ K, the osmotic water permeability, P_f, given in conventional unit of $cm \cdot s^{-1}$, and the above mentioned L^m are related by:

$$P_f = \frac{8.31 \cdot 10^2 \cdot 293 \cdot L^m}{18} = 1.353 \cdot 10^4 \cdot L^m \tag{28b}$$

RESULTS

Basic Analysis of the Problem

Two barriers delimit the lateral intercellular space of the present model: The tight junctions and the basal interspace membrane. In both membranes are the solute fluxes governed by the non-linear Hertz equation. A pump in the lateral membrane pumps solute into the *lis* and, dependent on properties of the delimiting membrane, may drive fluid absorption under equilibrium conditions. Before incorporating recirculation into this model, we will consider the simpler model of the *lis*, the two delimiting membranes, and the pump,

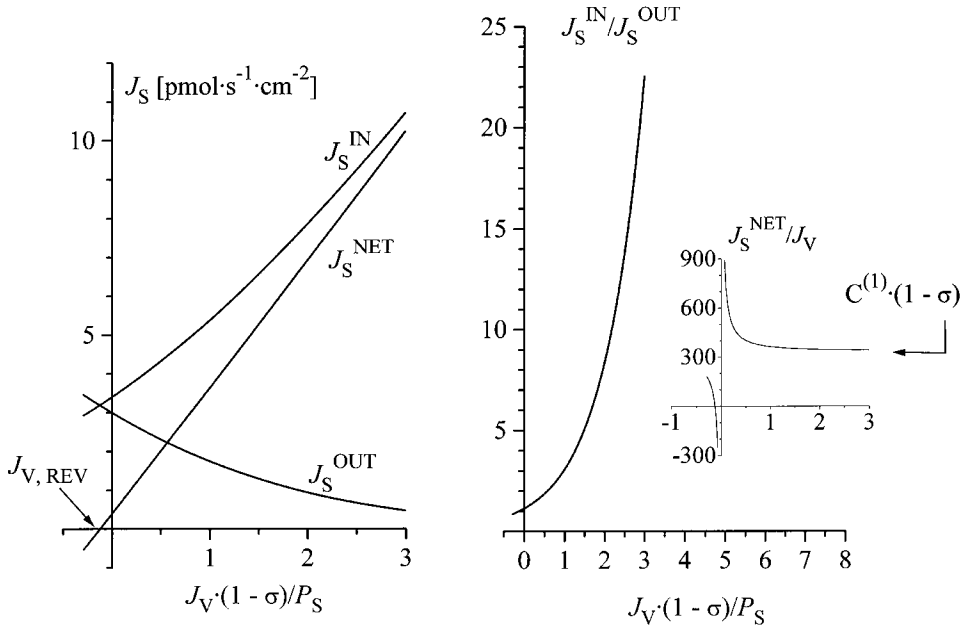

Figure 2. Convection-diffusion of solute, *S*, through a water permeable pore with reflection coefficient, σ. (Left) Function analysis of Hertz' equation giving relationship between solute flux, J_S, and water flux, $J_V \cdot (1 - \sigma)/P_S$, through the pore (Eq. 29). Included are also graphs of associated unidirectional fluxes, J_S^{IN} and J_S^{OUT} (see Eq. 30). In all computations P_S was kept constant, and $J_V \cdot (1 - \sigma)/P_S$ varied by varying J_V with $C^{(1)}$ = 340 mM, $C^{(2)}$ = 300 mM, and $\sigma = 10^{-5}$ (Eq. 29). With $J_V = 0$, the flux is governed by pure diffusion, $J_S = P_S \cdot (C^{(1)} - C^{(2)})$. Also the *x*-axis intercept ($J_S = 0$) is proportional with the diffusion permeability and given by, $J_{V,REV} = -[P_S/(1 - \sigma)] \cdot \log_e[C^{(1)}/C^{(2)}]$. (Right) Ratio of unidirectional fluxes increases steeply with increased imposed water flow through pore. (Inset) The slope of the asymptote of left-hand J_S-graph for $J_V \rightarrow \pm\infty$ is given by, $C^{(1)} \cdot (1 - \sigma)$. That is, in this limit transport of *S* is caused by convection, only.

and ask two questions: (a) What is the tonicity of the transportate? (b) What is the expected flux-ratio of a paracellular marker that traverses this system?

A single convection-diffusion barrier: The Hertz equation. We will start our analysis by considering the Hertz equation for a single convection-diffusion barrier and in the absence of solute pumping. With concentrations of the solute in compartment (1) and (2) denoted, $C^{(1)}$ and $C^{(2)}$, the Hertz equation reads:

$$J_S = J_V(1-\sigma^{bm})\frac{C^{(1)}\exp[J_V(1-\sigma)/P_S] - C^{(2)}}{\exp[J_V(1-\sigma)/P_S]-1} \qquad (29)$$

where J_S is the convection-diffusion flux through water filled pores with reflection coefficient, σ, solute permeability, P_S, and water flux, J_V. The unidirectional tracer fluxes (both positive) are then given by:

$$J_S^{1\rightarrow 2} = J_V(1-\sigma^{bm})\frac{C^{(1)}\exp[J_V(1-\sigma)/P_s]}{\exp[J_V(1-\sigma)/P_S]-1} \qquad (30a)$$

$$J_S^{2\rightarrow 1} = J_V(1-\sigma^{bm})\frac{C^{(2)}}{\exp[J_V(1-\sigma)/P_S]-1} \qquad (30b)$$

with a ratio of:

$$\frac{J_S^{1\rightarrow 2}}{J_S^{2\rightarrow 1}} = \frac{C^{(1)}}{C^{(2)}}\exp[J_V(1-\sigma)/P_S] \qquad (30c)$$

Fig. 2, left, depicts the net flux, Eq. 29, and the two unidirectional fluxes, Eqs. 30a and 30b, as function of $J_V \cdot (1 - \sigma)/P_S$. Fig. 2 (right) shows the flux-ratio, Eq. 30c, as function of $J_V \cdot (1 - \sigma)/P_S$. It is clear that the flux-ratio is a measure of $J_V \cdot (1 - \sigma)/P_S$, and that this quantity defines the degree to which convection dominates over diffusion. A solute flux-ratio in range of *e*, corresponding to measurements (Nedergaard et al., 1999), is compatible with a value of $J_V \cdot (1 - \sigma)/P_S \approx 1$ (assuming nearly the same concentration at the two sides of the membrane), i.e., with a flux of *S* which contains a significant diffusion component.

From Eq. 30 it is easily shown that, *lim* $J_S = P_S \cdot (C^{(1)} - C^{(2)})$ for $J_V \rightarrow 0$, which is pure diffusion.[3] In the alternative regime, pure convection, for $J_V \rightarrow \pm\infty$, *lim* $(J_S/J_V) = C^{(1)} \cdot (1 - \sigma)$ and $C^{(2)} \cdot (1 - \sigma)$, respectively. Whereas these features appear trivial mathematically, the physiological implications are not as trivial. As shown graphically in the insert of right hand panel of Fig. 2, in the regime where J_S and J_V are both positive and the flux of *S* contains a significant diffusion component, the concentration of the transportate, J_S/J_V, may obtain values much above $C^{(1)} \cdot (1 - \sigma)$. Since for $C^{(1)} > C^{(2)}$, J_S/J_V is monotonic decreasing, $J_S/J_V > C^{(1)} \cdot (1 - \sigma)$ for all finite values of J_V. Thus, with the generally low experimental ratio of paracellular unidirectional fluxes the concentration of the transportate would be significantly larger than $C^{(1)} \cdot (1 - \sigma)$. If we allow the (1)-side to represent the *lis* (which due to solute pumping fulfils $C^{lis} > C^i$), there is one value of σ, for which the fluid leaving the *lis* through the basement membrane would be isotonic. At higher values of σ, the absorbate would be hypotonic, at lower values, hypertonic. However, the value for σ at which isotonicity is obtained would be different for different values of J_V. Further, with a high value of σ

[3]Not only is the intersection with *y*-axis (Fick diffusion), but also the water flux, $J_{V,REV}$, at which $J_S = 0$, proportional with the solute permeability, i.e., $J_{V,REV} = -(P_S/[1 - \sigma]) \cdot \log_e[C^{(1)}/C^{(2)}]$.

the absolute fluid flow across the membrane for a certain hydrostatic pressure difference between *lis* and the inner compartment would decrease, Eq. 13. As we will see, solute recirculation allows isotonicity for a wide range of J_V while maintaining a low σ and hence a large fluid transport with modest p^{lis}.

Two serial convection-diffusion barriers. The above analysis applies formally only to a single convection-diffusion barrier described by Hertz equation, in our case either the tight junctions or the basement interspace membrane. The case of two serial barriers delimiting a middle compartment (*lis*) can be solved by applying Hertz equation for each of the two barriers, and eliminating the concentration in between (C^{lis}) to get the solute and water flux through the entire system. This was done by Patlak et al. (1963) who also included a solute pump facing the middle compartment. The equation equivalent to Eq. 29 in this case is (Patlak et al., 1963):

$$\frac{J_S}{J_V} = \frac{C \cdot [\exp(-\alpha_2) - \exp(\alpha_1)] + \frac{j}{J_V}\left[\frac{1-\exp(\alpha_1)}{1-\sigma_1}\right]}{\left[\frac{\exp(-\alpha_2)-1}{1-\sigma_1}\right] + \left[\frac{1-\exp(\alpha_1)}{1-\sigma_1}\right]} \quad (31)$$

where C is the concentration in both inner and outer bath (assumed to be the same), j is the (finite) rate of solute pumping into the middle compartment, σ_1 and σ_2 are the reflection coefficients for the first and second barrier, respectively, and $\alpha_1 = J_V(1-\sigma_1)/P_1$ and $\alpha_2 = J_V(1-\sigma_2)/P_2$, where P_1 and P_2 are the solute permeabilities of the first and second barrier, respectively. Considering the transported fluid, Patlak et al. (1963) showed that $\sigma_1 > \sigma_2$ defines water transport from the (1) to the (2) side, as one would expect. With this assumption, they showed that $J_V < j/(C\cdot(\sigma_1 - \sigma_2))$. They also showed that for all positive finite values of J_V, $J_S/J_V > (1-\sigma_2)\cdot C$. Thus, the problem of obtaining an isotonic fluid is the same for the two-membrane system as in the case of a single membrane.

Using the above strategy, Eqs. 30a and 30b, see also Eqs. 21, 22, and 25, can be used to derive an expression for the ratio of unidirectional fluxes across two serially arranged convection-diffusion barriers. The result is simply:

$$\frac{J_S^{1\to 2}}{J_S^{2\to 1}} = \frac{C^{(1)}}{C^{(2)}} \cdot \exp\left(\frac{J_V\cdot(1-\sigma_1)}{P_1} + \frac{J_V\cdot(1-\sigma_2)}{P_2}\right) \quad (32)$$

where now $C^{(1)}$ and $C^{(2)}$ are the concentrations at either side of the middle compartment (in Eq. 31 we assumed $C^{(1)} = C^{(2)} = C$). Thus for the case of a two-barrier system, the ratio of paracellular unidirectional fluxes is still a measure of the relative contribution of convection and diffusion.

The Recirculation Model

In the following we will consider the case of solute recirculation. If all membranes have non-zero hydraulic conductance, i.e., L^a, L^s, L^{tm}, L^{bm}, $L^{lm} > 0$, under transepithelial equilibrium conditions two pathways are available for transport of fluid across the epithelium. The one is the paracellular route with a water permeability governed by the hydraulic conductance of two membranes, L^{tm} and L^{bm}. The other is the translateral route with its water permeability governed by the hydraulic conductance of three membranes, L^a, L^{lm}, and L^{bm}. All membranes having a non-zero hydraulic conductance is here treated as the general case that will be dealt with in details immediately below. For this case, tight junction permeable solutes are transported by convection-diffusion across both tight junction and interspace basement membrane obeying principles outlined above in our basic analysis of two serial convection-diffusion barriers. In a subsequent section we discuss features of the model with eliminated tight junction hydraulic conductance, $L^{tm} \approx 0$, implying that solutes diffuse across tight junction with water entering the lateral coupling compartment via cells.

The Reference State

Choice of independent variables. With the results of our basic analysis in mind, the standard input variables were selected for obtaining a paracellular flux-ratio and absolute fluxes approximating those of Na^+ in toad small intestine, and an intracellular concentration of *S*, which amounts to less than 10% of its the mucosal concentration. In experiments with glucose in mucosal bath Curran (1960) showed that small intestine (rat ileum) transports water in proportion with Na^+ uptake, and that the absorbate always is isotonic with mucosal solution. Thus, parameter finding was done using version 2 of the model, i.e., isotonicity (300 mM) of the net absorbate was assumed. We selected a hydraulic conductance of the apical membrane of 10^{-7} $[(cm\cdot s^{-1})/(N\cdot cm^{-2})]$. This is equal to an osmotic water permeability of $1.35\cdot 10^{-3}$ $cm\cdot s^{-1}$ (Eq. 28b), and comparable with the estimate of the osmotic permeability of the brush border membrane of rat small intestine ($1.2\cdot 10^{-3}$ $cm\cdot s^{-1}$; Worman and Field, 1985). With no further experimental data, in the reference state we assume that the hydraulic conductances of the three plasma membranes scale to the relative membrane areas. If we assume that the cell is shaped like a cube, it will be appreciated that four sides are facing the *lis* and one side is facing each of the *i*- and *o*-compartments. Accordingly, $L^{lm} = 4\cdot L^a = 4\cdot L^s$. Since the lateral space of leaky epithelia exhibits large volume expansion upon stimulation of transepithelial volume absorption (Whitlock and Wheeler, 1964; Atisook et al., 1990), we apply similar scaling of compliance constants, $\mu^{lm} = 4\cdot\mu^a = 4\cdot\mu^s$. While our paracellular flux ratio analysis of small diffusible ions provides an estimate of the hydraulic conductance of the tight junction membrane (see

TABLE I

Values of Independent Variables of the Reference State with Non-Zero Hydraulic Conductance of All Five Membranes

Variable	Value	Variable	Value
Intensive variables			
C_S^a [mM]	300 mM	C_S^i	300
$\mathcal{C}_{ND}^a$ [mM]	0	$\mathcal{C}_{ND}^i$	0
Membrane parameters, solutes			
P_S^a [cm·s^{-1}]	$2.9\cdot10^{-6}$	P_S^a [cm·s^{-1}]	$5.574\cdot10^{-6}$ [cm·s^{-1}]
$J_S^{max,\,pump}$ [pmol·s^{-1}·cm·s^{-1}]	$8\cdot10^{3}$	(n = 3 sites on pump)	
P_S^{tm} [cm·s^{-1}]	$1.5\cdot10^{-6}$	P_S^{bm} [cm·s^{-1}]	$3.5\cdot10^{-5}$
$P_S^{tm,\,diff}$ [cm·s^{-1}]	0	$P_S^{bm,\,diff}$ [cm·s^{-1}]	0
Membrane parameters, water			
L^a (cm·s^{-1})·(N·cm^{-2})$^{-1}$	$1.0\cdot10^{-7}$	L^s (cm·s^{-1})·(N·cm^{-2})$^{-1}$	$1.0\cdot10^{-7}$
L^{lm} (cm·s^{-1})·(N·cm^{-2})$^{-1}$	$4.0\cdot10^{-7}$		
L^{tm} (cm·s^{-1})·(N·cm^{-2})$^{-1}$	$7.5\cdot10^{-7}$	L^{bm} (cm·s^{-1})·(N·cm^{-2})$^{-1}$	$7.5\cdot10^{-5}$
σ^{tm}	0.55	σ^{bm}	10^{-5}
Membrane parameters, compliant constants			
$\mu^{lm} = 4\cdot\mu^a = 4\cdot\mu^2$; $\mu^{cell} = \mu^{lm} + \mu^a + \mu^s$			

above), we have no data for choosing the value of the hydraulic conductance of the interspace basement membrane. To begin with, we assume a ratio of, $L^{bm}/L^{tm} = 100$. This would be compatible with the experimental analysis of isolated perfused renal tubule, indicating a hydraulic conductance of the tubular basement membrane, which is two to three orders of magnitudes greater than that of the (highly permeable) intact epithelial layer (Welling and Grantham, 1972). The resulting reference state is shown in Table I and Fig. 3, and in Table II are listed relevant measured fluxes of sodium ions in toad small intestine together with corresponding fluxes of *S* given by the model[4].

Before entering the analysis, regarding the choice of independent variables two points should be discussed. With glucose in bathing solutions, the ratio of transepithelial unidirectional Na^+ fluxes (considering in both directions the sum of cellular and paracellular fluxes) is similar for toad and rat small intestine (2–2.5). The fluxes of rat, however, are about three times larger than those of toad. For example, the transepithelial unidirectional influx in rat ileum is ~3,000 pmol·s^{-1}·cm^{-2} (Curran, 1960)[5] as compared with 1000 pmol·s^{-1}·cm^{-2} in toad (Nedergaard et al., 1999). It follows that the Na^+ conductance of the toad preparation is smaller than that of rat. Using the formula for the conductance, $G = P\cdot C\cdot F^2/(R\cdot T)$, with P being the permeability, C the concentration, and F, R, and T having their usual meanings, we calculate a tight junction resistance of the model of 585 Ω·cm^2, which is fairly large for a leaky epithelium. Frizzell and Schultz (1972) calculated the paracellular Na^+ resistance of rat small intestine to be 204 Ω·cm^2. This calculation made use of their experimental estimate of the paracellular unidirectional influx under transepithelial equilibrium conditions, $J_{NA}^{in,\,PARA} = 1361 \pm 250$ pmol·s^{-1}·cm^{-2}, by assuming that the flux was due to diffusion, only. But as this component most likely is due to convection-diffusion, it is expected to be larger than the pure diffusion flux. Thus, the value of 204 Ω·cm^2 is expected to be an underestimate. In the calculations immediately below we wish to simulate the toad preparation, for which we have estimates of the recirculation flux. Therefore, the somewhat low tight junction permeability of $P_S^{tm} = 1.5\cdot10^{-6}$ cm·s^{-1} has been chosen together with an interspace basement membrane permeability, $P_S^{bm} = 3.5\cdot10^{-5}$ cm·s^{-1}. This latter permeability would correspond to a resistance of 23 Ω·cm^2, which is similar to the experi-

TABLE II

Experimentally Obtained Na^+ Fluxes in Toad Small Intestine Compared with Fluxes of the Driving Species Given by Model*

	J^{NET}	J_{ms}^{para}	J_{sm}^{para}	$\frac{J_{ms}^{para}}{J_{sm}^{para}}$	$\frac{-J_S^{\S}}{J_S^{pump}}$
Experiment‡	773 ± 56	450 ± 40	130 ± 20	3.66 ± 0.34	0.65 ± 0.03
Reference state	1275	725	211	3.44	0.66
Pseudo solvent drag§	756	433	375	1.15	0.71

*All fluxes are in pmol·s^{-1}·cm^{-2}.

‡Mean ± SEM of five preparations, from Nedergaard et al., 1999.

§Tight junction hydraulic conductance, $L^{tm} \approx 0$.

[4]The driving solute in small intestine is the charged sodium ion. As explained in Discussion, in this first version of the mathematical model, we have replaced the sodium ion with a diffusible non-electrolyte in order to simplify and generalize the treatment. In comparing our model with experimental data we shall nevertheless draw on measured electrolyte fluxes for identification of physiologically relevant areas of parameter space.

[5]Similar fluxes were obtained by Frizzell and Schultz (1972), and they refer to in vitro studies. The fluxes of Na^+ measured in vivo (Curran and Solomon, 1958) are larger by a factor of two when compared to in vitro.

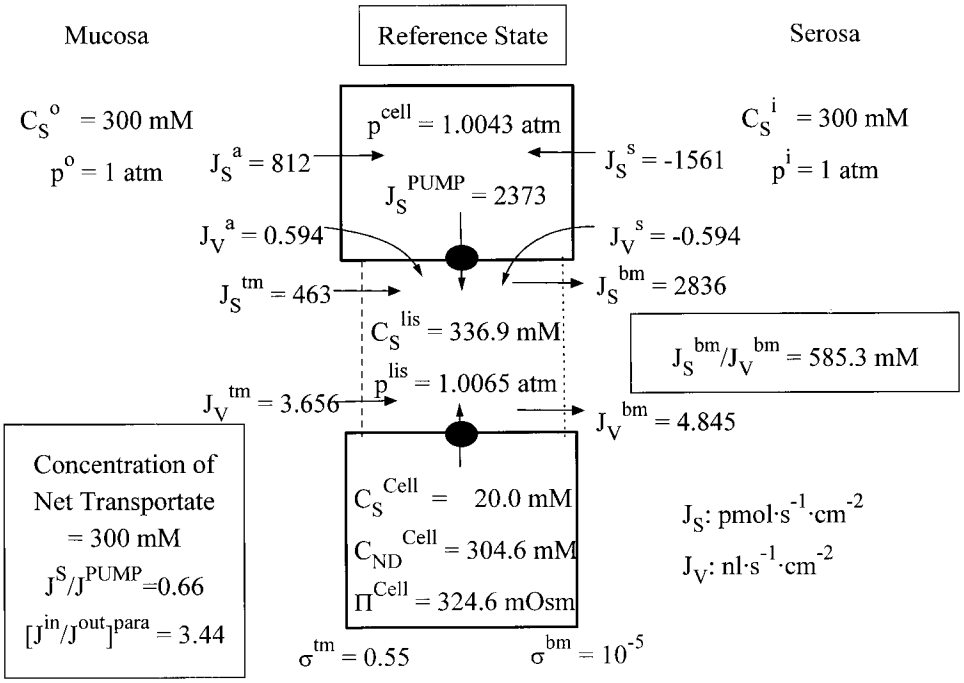

Figure 3. Reference state of the recirculation model. Shown are computed stationary fluxes, concentrations, and hydrostatic pressures with independent variables listed in Table I. Note that calculated concentration of the fluid appearing downstream lateral space is strongly hypertonic, J_S^{bm}/J_V^{bm} = 2836/4.845 = 585.3 mM. With concentration of the net transportate, J_S^{NET}/J_V = $(J_S^{bm} - J_S^s)/(J_V^{bm} - J_V^s)$, being 300 mM, i.e., identical with concentration of bathing solutions, the fraction of the pump flux, which is derived from the inner compartment, is, $-J_S^s/J_S^{ump}$ = 1561/2373 = 0.658 (left hand inset). Isotonic transport is achieved with moderate excess concentration (336.9 − 300 = 36.9 mM) and pressure (1.0043 − 1 = 0.0043 atm) of lateral intercellular space and a relatively small paracellular flux ratio, with the latter being compatible with that of toad small intestine (Table II). (Bottom right) In this and all other figures are solute fluxes in pmol^{-1}·s^{-1}·cm^{-2} and water fluxes in nl·s^{-1}·cm^{-2}.

mental estimate of 22 Ω·cm^2 of toad gallbladder (Hénin et al., 1977). In some later calculations we extend the analysis to epithelia with much higher fluxes. The other point worth mentioning here is that in the model, and toad intestine, are the paracellular fluxes significantly smaller than those passing the cells (Fig. 3). This was also reported by Frizzell and Schultz (1972), who found that both at high (140 mM) and low (28 mM) mucosal [Na^+] is the paracellular unidirectional Na^+ influx no more than one third of that passing the cells (short-circuited rat ileum). This need not be incompatible with the notion of a transepithelial conductance dominated by a leaky shunt, since this refers to electrical measurements. If the cellular fluxes are carried predominantly by electro-neutral transporters, they are not expected to contribute to the electrical conductance of the epithelium.

Features of the reference state. With non-zero water permeability of all membranes and similar hydrostatic pressure (1 atm) and concentrations (300 mM) of external compartments, the hydrostatic pressure of the cell, p^{cell} = 1.0043 atm, while the sum of concentrations of diffusible and non-diffusible solutes of the cell is 324.6 mM (Fig. 3). This latter value amounts to a measurable hyperosmolality (8.2%) of the cellular compartment. With trans-lateral water flux the major determinant of the steady state cellular hyperosmolality is the hydraulic water permeability of the plasma membranes, which here is assumed to be fairly low. It is not a surprising result that the osmotic concentration of the cell drops to near that of the external solutions if either L^a or L^s, or both, are increased. For example, the total osmotic pressure of the cells would be ∼308.5 mM if L^a and L^s are increased by a factor of five, and this results in minor changes, only, of all other dependent variables of the reference state (not shown). If the hydraulic conductance of the lateral membrane is set to zero (L^{lm} = 0), the translateral water flux is abolished so that the total osmotic pressure of the cell drops to 300.16 mM with a hydrostatic pressure of, p^{cell} = 1.0044 atm. With all other independent variables kept at their reference values, neither does this maneuver result in any significant change of the reference state's dependent variables indicated in Fig. 3 (calculations not shown). We return to the question about the significance of the plasma membranes' water permeability in the discussing of uphill water transport.

At steady state the flux of water from the outer solution into the lateral intercellular space is accomplished by the concentration of *S* of the lateral intercellular space (336.9 mM) being larger than that of the outer solution (300 mM), that is, C_S^{lis}/C_S^s = 1.12. Likewise, the excess hydrostatic pressure of *lis*, which provides the driving force for moving water into the inner compartment, is in range of plausible values, $p^{lis} - p^i$ = 6.5 cm H_2O. This particular mathematical solution is governed by, P_S^{bm} = 3.5·10^{-5} cm·s^{-1}. Thus, with $J_V^{bm}(1-\sigma^{bm})/P_S^{bm}$ = 4.845·10^{-6}·(1 − 10^{-5})/3.5·10^{-5} = 0.138, the flux of *S* through water pores of the interspace basement membrane contains a significant diffusion component (see

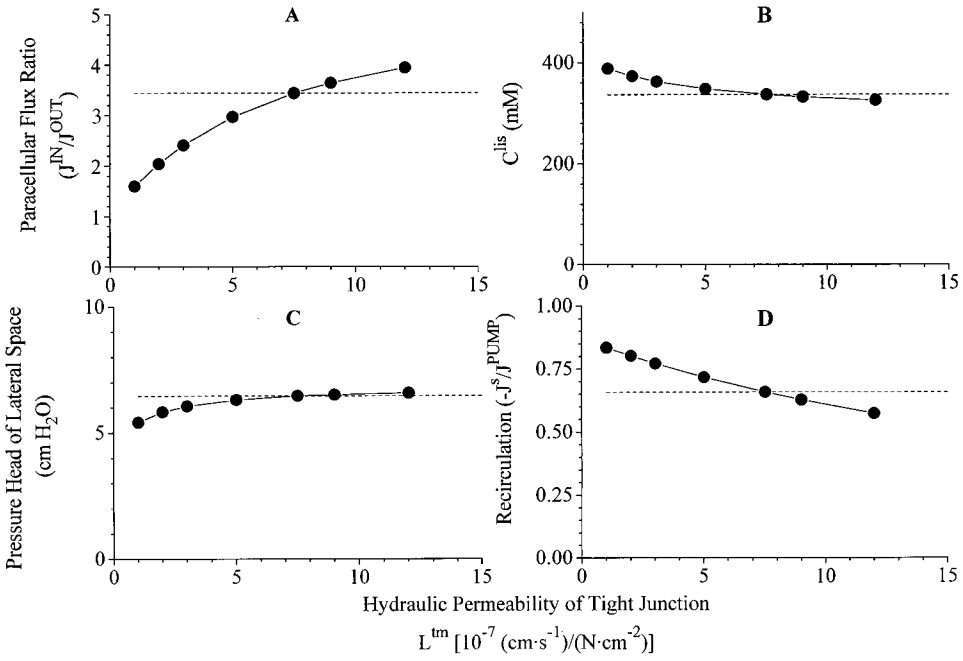

Figure 4. Robustness of computations I. The strongly coupled non-linear equations provide mathematical solutions with dependent variables varying monotonically about the chosen reference state. Here are shown variations of, (A) paracellular flux-ratio, (B)concentration of *S* in lateral intercellular space, (C) pressure head, $p^{lis} - p^{bath}$, of lateral intercellular space, and (D) the relative recirculation flux, when hydraulic permeability of tight junction is varied more than an order of magnitude. Dashed lines indicate corresponding values of reference state. Compare with Figs. 5, 6, 7, and 8.

Fig. 2). As a result, the virtual concentration of the transportate emerging downstream the lateral space, J_S^{bm}/J_V^{bm} = 2836/4.845 = 583.3 mM, is significantly larger than the steady state concentration of the lateral intercellular space fluid (336.9 mM)[6]. With the restriction of net isotonicity of the absorbate, $(J_S^{bm} + J_S^{\S})/(J_V^{bm} + J_V^{\S})$ = 300 mM, our mathematical solution gives a stationary uptake of *S* across the serosal cell membrane, $J_S^{\S}$ = −1561 pmol·s^{-1}·cm^{-2}. This means that 66% of the molecules pumped through the lateral membrane is derived from the inner compartment ($-J_S^{\S}/J_S^{ump}$ = 1561/2373 = 0.658), which is in accord with the estimate obtained in experiments with toad small intestine (Table II).

Robustness of mathematical solutions. With only five dependent parameters measured at this stage (Table II), the model is of course underdetermined, and it follows that the reference state of Fig. 3 is only one of many that could be constructed to be consistent with the data. However, if the mathematical model provides faithful solutions to our physiological problem the qualitative behavior of the model should not be sensitive to exact values of variables of the input list. In other words, in the neighborhood of each independent variable listed in Table I, also new sets of mathematical solutions should be compatible with the reference state. We have investigated this by examining how paracellular flux-ratio, C_S^{lis}, p^{lis}, and recirculation flux vary with imposed variations of tight junction reflection coefficient, interspace hydraulic conductivities, and solute permeabilities. In doing this we used version 2 of the model, so that serosal membrane solute permeability and hence recirculation flux would all the time be adjusted for achieving net isotonicity of the absorbate. Effects of varying tight junction properties are depicted in Figs. 4–6, which will be discussed together. As mentioned above (Fig. 2), increasing the ratio, $J_V(1 - \sigma)/P_s$, leads to increase of the flux-ratio of solutes passing water permeable pores. Because an increase of L^{tm}, or a decrease of σ^{tm}, result in an increase of J_V^{tm}, for relatively small values of L^{tm} the paracellular flux-ratio becomes a monotonic increasing function of L^{tm} (Fig. 4 A), and a monotonic decreasing function of σ^{tm} (Fig. 5 A). Decreasing P_S^{tm} has the effect of reducing the diffusion component of J_S^{tm} and, thus, increasing the flux-ratio (Fig. 6 A). The force driving water across tight junction is given by the difference in effective osmotic pressure between lateral intercellular space and outer (mucosal) compartment (Eq. 12). Thus, decreasing hydraulic water permeability (Fig. 4 B), or reflection coefficient (Fig. 5 B), result in new steady states with increased C_S^{lis}. Mathematical solutions providing physiologically relevant flux-ratios also provide plausible values of C_S^{lis}, i.e., $C_S^{lis}/C_S^{bath} < 1.30$. In the above ranges of the three independent variables, also interspace hydrostatic pressure (Figs. 4 C, 5 C, and 6 C) and recirculation flux (Figs. 4 D, 5 D, and 6 D) exhibit shallow monotonic variation about the reference state. In conclusion, by letting each of the three independent variables, L^{tm}, σ^{tm}, and P_S^{tm} span almost a decade, mathematical solutions are obtained which are qualitatively similar to the reference state.

[6]Note that the diffusive component of *S* discussed here is that of convection-diffusion pores. The diffusion permeability of interspace channels with no water permeability is zero in the model's reference state (Table I).

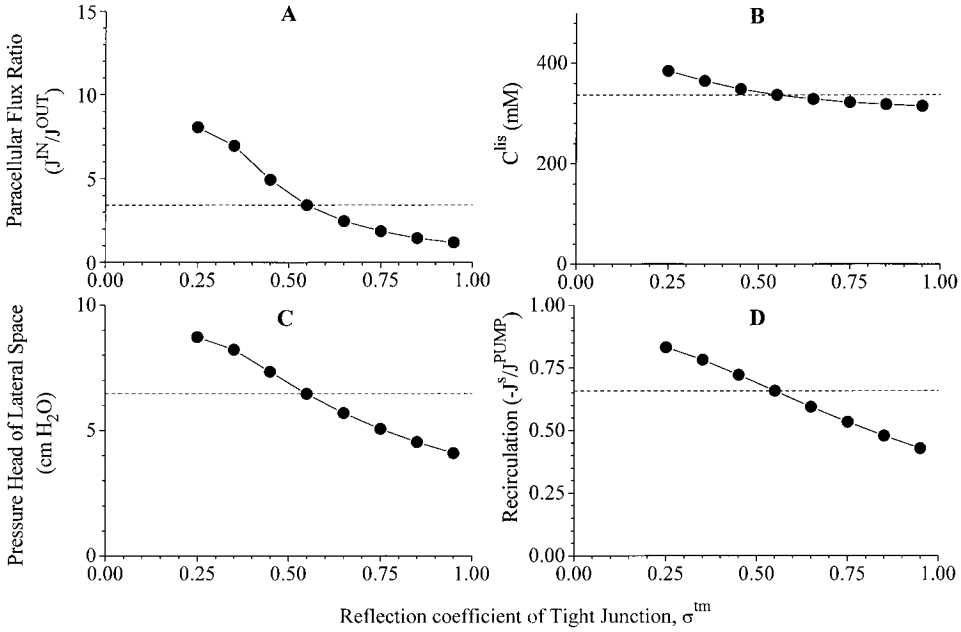

Figure 5. Robustness of computations II. Here are shown variations of same dependent variable as in FIGS. 4, 6, 7, and 8, when tight junction reflection coefficient is varied from 0.25 to 0.95. Dashed lines indicate corresponding values of reference state.

It is as expected that interspace and cellular hydrostatic pressures are the only dependent variables that are significantly influenced by changes of the hydraulic permeability of interspace basement membrane (Fig. 7). Thus, while $p^{lis} - p^{bath}$ varies from 48.2 to 4.05 cm H_2O (Fig. 7 C), $p^{cell} - p^{bath}$ varies in parallel from 32.1 to 2.70 cm H_2O (not shown). The corresponding variation of C_{ND}^{cell} is trivial, from 305.4 to 304.5 mM (not shown). The interspace hydrostatic pressure also increases with increasing interspace basement membrane reflection coefficient, σ^{bm} (not shown). This is because the effective osmotic force directed from inner compartment to interspace increases with the reflection coefficient (Eq. 13). With virtually unchanged volume flow the increase of p^{lis} compensates for this increase of the counteracting osmotic force. As discussed above, the concentration of the fluid emerging from lateral intercellular space is much sensitive to the solute permeability of the basement membrane and, pari passu, so is the recirculation flux (Fig. 8 D). However, it is worth noting that no dramatic effects are observed by varying P_S^{bm} within an order of magnitude. At any of the chosen values of this parameter is isotonic transport achieved by recirculating a significant proportion of the pumped solute flux.

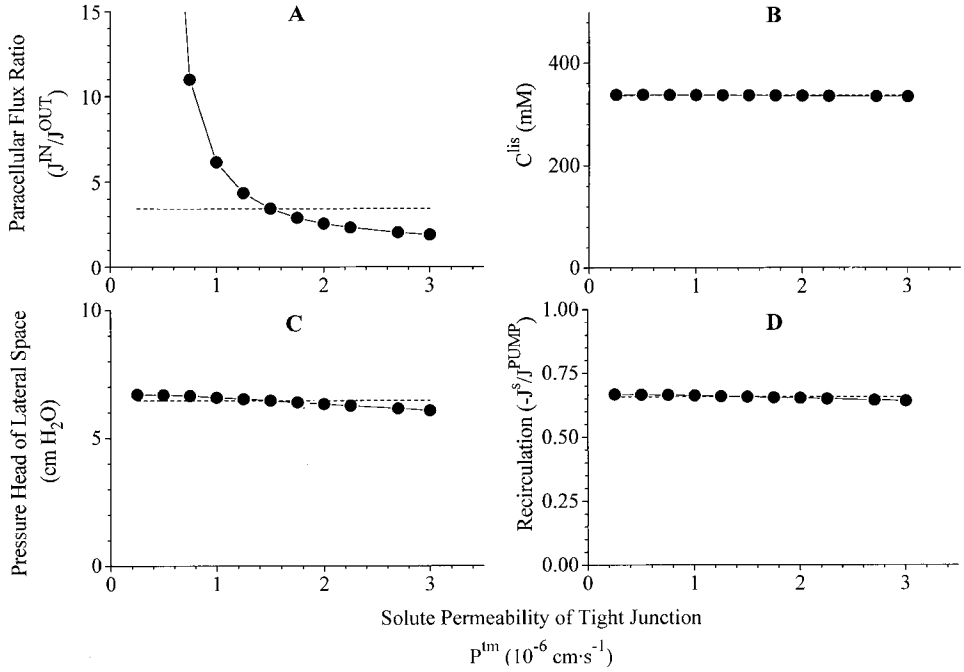

Figure 6. Robustness of computations III. Variations of same dependent variable as in FIGS. 4, 5, 7, and 8, when solute permeability of tight junction is varied more than an order of magnitude. Dashed lines indicate corresponding values of reference state.

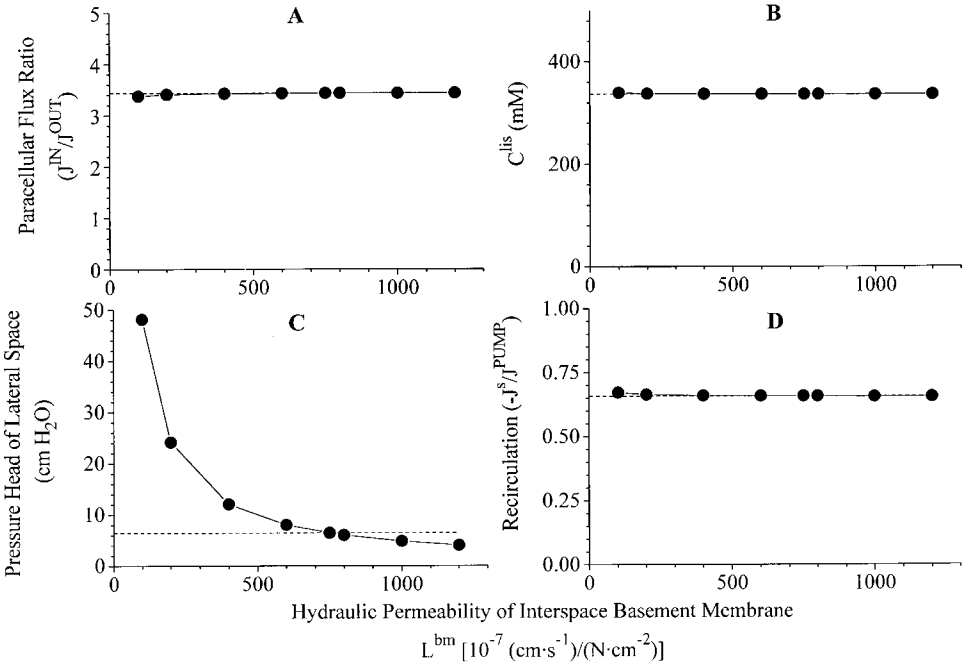

Figure 7. Robustness of computations IV. Variations of same dependent variable as in FIGS. 4, 5, 6, and 8, when hydraulic permeability of interspace basement membrane is varied more than an order of magnitude. Dashed lines indicate corresponding values of reference state.

Significance of solute recirculation. The reference state was found with two independent requirements. (a) Permeabilities were selected for reproducing solute fluxes compatible with measured Na^+ fluxes in toad intestine. (b) We asked for a mathematical solution containing an isotonic net transportate (version 2 with Eq. 27 and *TON* = 300 mM). Therefore, the fairly large recirculation flux given by the model (~0.7), which is shown above to be a robust result, is a derived quantity. The experimental analysis resulted in an estimate of similar magnitude (Table II). Thus, the computed result indirectly verifies the hypothesis of the experimental paper that recirculation is of significance for maintaining isotonic transport. For exploring this feature in more detail we computed the tonicity of the transportate as a function of the recirculation flux. This was achieved with version 1 (containing Eq. 26) by varying serosal permeability ($P_{\S}$) about the value listed in Table I. From the results shown in Fig. 9 A it can be seen that even with tonicities of the net transportate ranging within ± 15%

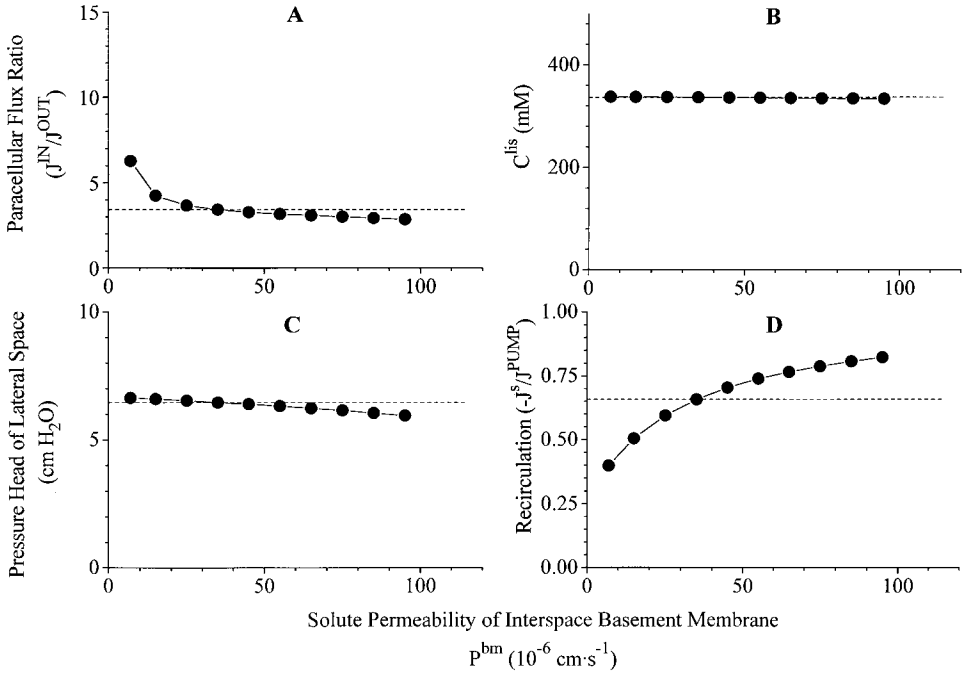

Figure 8. Robustness of computations V. Variations of same dependent variable as in FIGS. 4, 5, 6, and 7, when solute permeability of interspace basement membrane is varied more than an order of magnitude. Dashed lines indicate corresponding values of reference state.

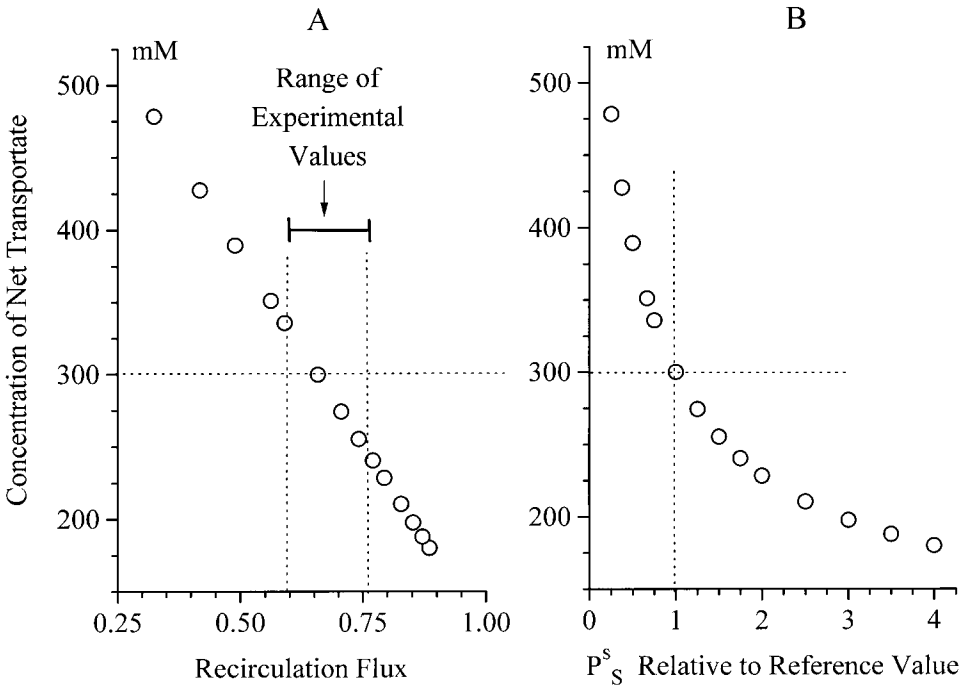

Figure 9. Significance of solute recirculation for the tonicity of the net transportate. (A)Computed tonicity of the net transportate as function of the recirculation flux. Near isotonic transport is predicted for the range of experimentally determined recirculation fluxes. (B) The variation of the tonicity of the net transportate was achieved by varying the solute permeability of the serosal membrane, see Eq. 26 of text.

of the tonicity of the bathing solutions is there a very significant recirculation flux. This range is covered by values of P_S^s that are within $\times 0.67$ and $\times 1.5$ the standard value (Fig. 9 B). Since the tonicity of the transportate of toad intestine was not measured, the exact value of the permeability of the recirculation pathway cannot be inferred from these computations. For investigating the explanatory range of the model, in computations requiring use of version 2 we decided to set $TON = 300$ mM. But as the analysis above showed that neither is the behavior of the model dependent on exact values of input variables nor is it of critical importance whether we run the model under assumption of truly isotonic or near isotonic transport, results obtained with the above choice are expected to apply more generally for epithelia that may generate a near isotonic transportate.

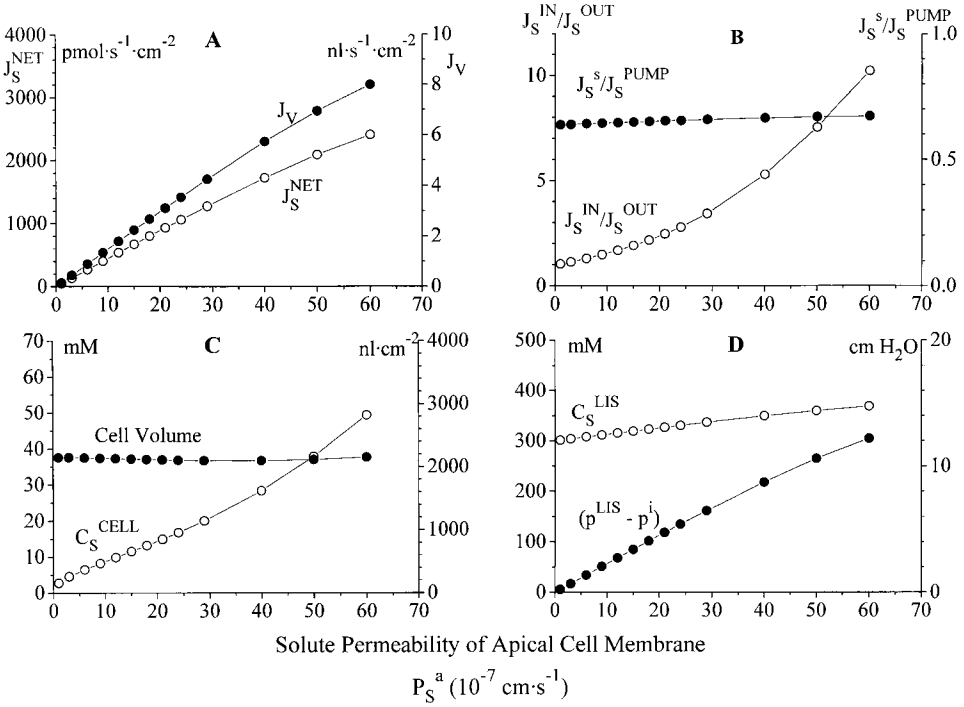

Figure 10. The major fraction of solute entering inner compartment has passed the cells. (A) The volume flow of an isotonic transportate increases with the apical membrane's solute permeability, and thus the flux of *S* across the apical membrane (saturation is due to saturation of pump flux). These fluxes are obtained with supposedly physiologically realizable values of (B) paracellular flux ratio and recirculation flux, (C) cell volume and concentration of driving solute in cell, and (D) concentration and hydrostatic pressure of lateral intercellular space.

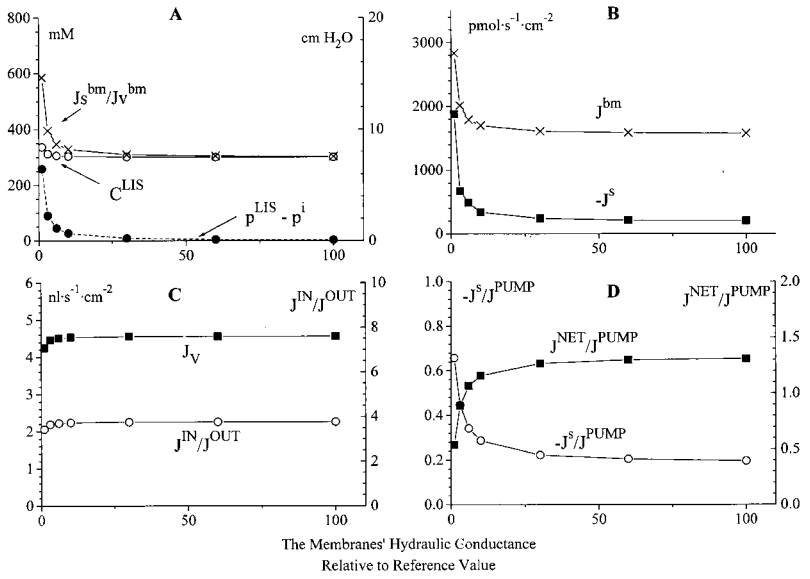

Figure 11. Energetic efficiency of isotonic transport depends on hydraulic conductance. All five hydraulic conductances were increased, and by the same factor. (A) With increasing water permeability the driving force for transjunctional and transcellular water transport decrease, that is, the excess concentration of the lateral intercellular space decrease. Thus, the concentration of the fluid emerging downstream the lateral space approaches that of bathing solutions. (B) This is also indicated by a significant decrease of the flux emerging downstream the lateral space (J^{bm}), and a diminished demand on recirculation ($-J^{s}$). (C) Volume flow is little affected by hydraulic permeability of the transjunctional and transcellular pathways, and neither is paracellular flux ratio. (D) As a result, with increasing hydraulic conductance the energetic efficiency of isotonic transport is increased.

Rate Limiting Steps of Isotonic Volume Flow

Varying apical membrane solute permeability. In the computations shown in Fig. 10 the translateral flux of *S* was varied by varying solute permeability of the apical cell membrane. The stationary flux of the isotonic transportate is indicated by the net solute flux, J_S^{net}, and the water flux, J_V, with, J_S^{net}/J_V = 300 mM (model version 2). It can be seen that in the recirculation model is the transepithelial paracellular flux of water, J_V, driven by the transcellular active solute flux with *S* being derived from mucosal solution (Fig. 10 A). The paracellular flux ratios are within the physiological range with the relative recirculation flux ($-J_S^{s}/J_S^{ump}$) being virtually unaffected (Fig. 10 B). In Fig. 10 C is shown that the large variation of the fluxes of water and solutes in the model are accomplished with little variation of cell volume. The associated interspace parameters (Fig. 10 D) exhibit somewhat larger variations, but both are probably being kept within realizable values.

Significance of hydraulic conductance. Thus, in the recirculation model, the rate of active solute transport is governing the transport of water through the epithelium. The coupling of the solute and water fluxes takes place in the lateral interspace, with direction of water flow determined by the relative values of the two reflection coefficients, that is, $\sigma^{tm} > \sigma^{bm}$ directs absorption. It would be of interest, therefore, to analyze effects of varying the hydraulic conductance of the epithelium on transepithelial solute and water flows (Fig. 11). In these computations, with their relative magnitudes maintained the five hydraulic conductances were increased, while all other independent variables were kept at their reference state values (Table I). By increasing the hydraulic conductance, C^{lis} and the virtual concentration of the fluid emerging from lateral space, J_S^{bm}/J_V^{bm}, both approach the concentration of bathing solutions (Fig. 11 A). Concomitantly the solute flux of *S* emerging from the lateral space, J_S^{bm} and, pari passu, the recirculation flux, $-J_S^{s}$ (Fig. 11 B), are diminished. Thus, the response to an increase of the hydraulic conductance is a diminished driving force for the flux of water with the volume flow kept within a narrow range about its reference state of 4.2 nl·s^{-1}·cm^{-2} (Fig. 11 C). It follows, that the paracellular flux ratio of the driving solute is also kept within a narrow range (Fig. 11 C). The physiological significance of this is that solute transport becomes energetically more effective as indicated by the increase of J_S^{net}/J_S^{ump} (Fig. 11 D). With the individual hydraulic conductances of ×10 their reference values, the fluxes entering the calculation are: The flux into the interspace from cells via the pump and from the outer solution via tight junction is, 1176.2 and 523.9 pmol·s^{-1}·cm^{-2}, respectively. With cellular reuptake of –338.6 pmol·s^{-1}·cm^{-2}, we thus obtain, J_S^{net}/J_S^{ump} = (1176.2 + 523.9 – 338.6)/1176.2 = 1.16. The general conclusion is that for a solute pump driving a transepithelial water flow, the thermodynamic efficiency can be higher than that of the pump itself. It is noted that the above extra solute flux of 185.3 pmol·s^{-1}·cm^{-2} is due to the pump-driven paracellular convection-diffusion flux being larger than the recirculation flux. For the sodium pump this would imply that more than 3 Na^+ are transported across the epithelium per ATP molecule split by the Na^+/K^+-ATPase. This interesting feature of the model shall be explored in more detail below.

Significance of solute-pump density. Under transepithelial equilibrium conditions is the transepithelial water flux governed by the apical permeability of the driving solute implying that volume flow saturates with saturation of the lateral solute pumps (Fig. 10 C). Further-

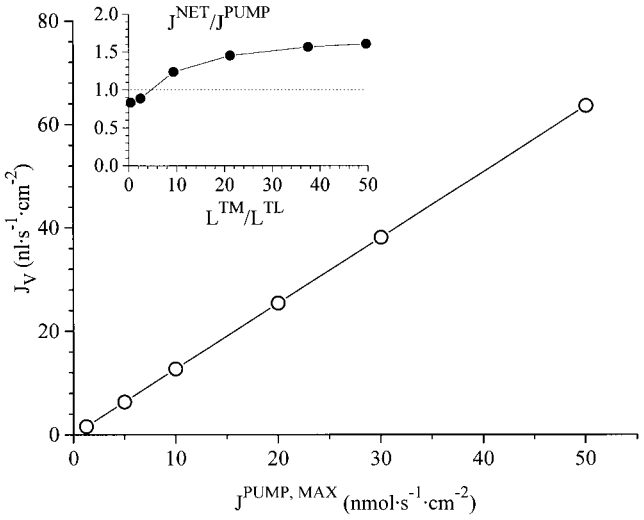

Figure 12. Rate of isotonic transport varies with solute flux through cells (see also FIG. 10), here accomplished by varying pump density on lateral intercellular space membrane (under conditions of near-constant intracellular concentration of driving solute, not shown). Water fluxes shown here span the range obtained with amphibian leaky epithelia (few nl·s^{-1}· cm^{-2}) to the very active rat proximal tubule (40–60 nl·s^{-1}· cm^{-2}). *Inset*: If the major component of water uptake takes place via tight junction, the energetic efficiency is high. With mitochondrial P/O ratio of 3, an efficiency of, $J^{NET}/J^{PUMP} = 1.5$, would correspond to 27 moles Na^+ transported for each mole of O_2 consumed by activity of sodium pump in accord with mammalian kidney (see Discussion). The model can produce this result with transjunctional hydraulic conductance (L^{tm}) being an order of magnitude larger than the translateral hydraulic conductance [$L^{tl} = L^a \cdot L^{lm}/(L^a + L^{lm})$].

more, increasing the hydraulic conductance of the epithelium increases the energetic efficiency of coupling between solute and water fluxes with very minor effect on the transepithelial water flux (Fig. 11, C and D). Among vertebrate (kidney) epithelia isotonic volume reabsorption is varying more than one order of magnitude from ~1 nl·s^{-1}·cm^{-2} in amphibian kidney (e.g., Whittembury and Reuss, 1992) to 30–60 nl·s^{-1}·cm^{-2} in mammalian kidney (e.g., Weinstein, 1992) with the associated osmotic water permeability spanning two decades, from ~$0.5 \cdot 10^{-2}$ in *Necturus* proximal tubule (Benzel et al., 1968) to ~0.5 cm·s^{-1} in rabbit proximal straight tubule (Schafer et al., 1978). The latter value is ~370 times larger than the overall osmotic permeability of the reference epithelium (see below, Fig. 13). We will here explore whether the recirculation model may cover a similar range when density of pumps on the lateral intercellular space membrane is varied. In these computations, for emphasizing the significance of the active solute flux, only the density of pumps on the lateral membrane and the apical membrane's diffusion permeability are varied (with their ratio staying constant for achieving a virtually constant C_S^{cell} of ~20 mM). For obtaining, at large transport rates, physiologically realistic interspace parameters and paracellular flux ratios, the interspace membrane permeabilities were set to values ×10 that of their respective reference values, and all hydraulic conductances were increased by a factor of 200 relative to those of the reference state, that is, placed within the upper range of mammalian values discussed above. Fig. 12 shows that by varying pump density by a factor of 40, computed isotonic fluid absorption spans the range of 1.6–64 nl·cm^{-2}·s^{-1} corresponding to the above physiological range of vertebrate proximal tubule.

In the computations shown in the inset of Fig. 12 the volume flow across the epithelium was maintained at about the same value (~60 nl·cm^{-2}·s^{-1}), while the ratio of transjunctional and translateral hydraulic conductance, L^{tm}/L^{tl}, was varied (translateral hydraulic conductance, $L^{tl} = L^a \cdot L^{lis}/[L^a + L^{lis}]$). Large energetic efficiencies of transepithelial active solute transport is being obtained with large ratio of L^{tm}/L^{tl}, and with an unmeasurable small osmotic concentration difference between bath and lateral intercellular space (303.2 mM ⩾ $C_S^{lis} - C_S^{bath}$ ⩾ 301.5 mM, not shown). An efficiency of $J_S^{net}/J_S^{pump} \approx 1.5$ would be in accord with mammalian proximal tubule (see Discussion). It is seen that this high efficiency of the model is associated with a transjunctional hydraulic conductance that is at least an order of magnitude larger than the hydraulic conductance of the translateral pathway.[7] Even under these conditions can the recirculation flux be significant (for $L^{tm}/L^{tl} = 37.5$ is $J_S^{net}/J_S^{pump} = 1.57$, and $-J_S^{s}/J_S^{pump} = 0.11$). If σ^{tm} is increased, e.g., to 0.85, the recirculation flux is being decreased to a small value (see Fig. 5). But as the tight-junction convection-diffusion flux also decreases, the energetic efficiency becomes smaller (calculations not shown). The general conclusion is that in a compartment model like the one presented based on simple convection-diffusion theory, an energetic efficiency of solute transport larger than that of the pump itself requires a relatively large flow of water through convection-diffusion pores of tight junction.

Effect of varying ambient osmolality. Since the osmolality of the net transportate (*TON* in Eq. 27) can be set to that of the bathing solutions it follows that the model can produce an isotonic absorbate whatever ambient osmolality is chosen. Thus, the model directly reproduces the finding that rabbit gallbladder transports fluid with a tonicity approximating that of the bathing solution used (Diamond, 1964b; Whitlock and Wheeler, 1964).

[7]Note that despite the transjunctional and the translateral water flux is governed by a similar driving force, is the ratio of these fluxes smaller than the ratio of the hydraulic conductances of the two pathways (L^{tm}/L^{tl}). This follows from the necessary condition that the reflection coefficient of the tight-junction convection-diffusion channel is less than unity.

TABLE III

*Computations with Varying External Osmolality**

$C_S^o = C_S^i = J_S^{net}/J_V$	$-J_S^s$	J_S^{tm}	$\frac{J_S^{net}}{J_S^{ump}}$	J_S^{ump}	C_S^{lis}	J_V
mM	*pmol·s⁻¹·cm⁻²*	*pmol·s⁻¹·cm⁻²*		*pmol·s⁻¹·cm⁻²*	*mM*	*nl·s⁻¹·cm⁻²*
50	518	236	0.67	859	51.4	11.5
100	578	536	0.97	1301	102	12.6
200	631	1140	1.24	2121	202	13.2
300	666	1744	1.37	2922	302	13.3
400	696	2344	1.44	3712	402	13.4
500	724	2939	1.49	4493	502	13.4
600	749	3525	1.53	5262	602	13.4

Ambient concentration of *S* is indicated in column 1; computations were carried out with tonicity of the net transporate (J_S^{net}/J_V) set to similar value (*TON* of Eq. 27). Computed transepithelial water flux (J_V) and energetic efficiency of solute transport (J_S^{net}/J_S^{ump}) approach those of rabbit gallbladder at ambient osmotic concentrations of 300 mM. For fulfilling these requirements together with a physiological cellular concentration of *S* (C_S^{cell} = 18.0 mM) and a paracellular flux ratio of *S* of ∼2, the independent variables were adjusted to $J_S^{ump,\,max} = 11{\cdot}10^3$ pmol·s^{-1}·cm^{-2}, $J_S^g = 8{\cdot}10^{-6}$ cm·s^{-1}, plasma membrane hydraulic conductances increased ×10 with respect to their values given in Table 1, $L^{tm} = 6{\cdot}10^{-6}$ (cm·s^{-1})·(N·cm^{-2})$^{-1}$, $L^{bm} = 6{\cdot}10^{-4}$ (cm·s^{-1})·(N·cm^{-2})$^{-1}$, $P_S^{tm} = 1.5{\cdot}10^{-5}$ cm·s^{-1}, $P_S^{bm} = 3.5{\cdot}10^{-5}$ (cm·s^{-1})·(N·cm^{-2})$^{-1}$, with the other input variables as indicated in Table I.

In the computations shown in Table III the concentration of the external compartments was changed in a symmetrical way using version 2 of the model ($C_S^g = C_S^i = J_S^{net}/J_V$) with the input parameters adjusted so that computed volume flow and energetic efficiency of solute transport are similar to those of rabbit gallbladder, i.e., J_V = 11–14 nl·s^{-1}·cm^{-2} (Diamond, 1964b) with a cost of transport of 24 mole Na^+ / mole O_2 (Martin and Diamond, 1966), see legend of Table III. A reduction of external solute concentration (column 1) results in lowering of solute fluxes and, therefore, also in a reduced recirculation flux for maintaining an isotonic absorbate (column 2). With decreasing mucosal concentration of *S* also the paracellular convection flux of *S* is decreasing (column 3). As discussed in detail above, with a relatively high energetic efficiency of solute transport in gallbladder, the recirculation flux would have to be relatively small, while the paracellular convection flux is relatively high. Because the large convection flux decreases much more than the small recirculation flux, the overall efficiency of solute transport is predicted to decrease significantly with decreasing external osmolality (column 4). With a high energetic efficiency at physiological conditions, this is a robust result and it is confirmed by an experimental study relating oxygen consumption to net Na^+ transport in rabbit gallbladder (Frederiksen and Leyssac, 1969; see Discussion).

As the cellular solute concentration decreases with decreasing ambient concentration (not shown), the pumped flux of *S* is being reduced (column 5), and so is the concentration of the lateral intercellular space (column 6). As a result, the driving force for transporting water from the outer bath into the lateral intercellular space remains virtually constant. Therefore, the transepithelial volume flow does not change significantly upon dilution of the bathing solutions (column 7). This is not confirmed by experiments with gallbladder, which showed a significantly increased volume flow with decreasing ambient osmolality (Diamond, 1964b; Frederiksen and Leyssac, 1969). With reference to computed results presented in the sections above, better agreement between computations and experiments would be obtained if the pumped flux is being activated in preparations exposed to diluted bathing solutions. However, with no further evidence for such a regulation this suggestion remains speculative.

Water Transport in Presence of Transepithelial Osmotic Gradients

Uphill water transport. Increasing the mucosal osmolarity by adding a non-permeable solute to the outer bath results in diminished steady state water fluxes across the two apical barriers, and eventually these fluxes become "backward". Thus, at some point net water flow reverses, switching the epithelium from net absorption to net secretion, which makes adjustment of the osmolarity of transport via recirculation meaningless. Therefore, in performing these strength of transport calculations we used version 1 of the model, in which mucosal osmolarity was raised under conditions of unchanged recirculation permeability. It can be seen from the computed results in Fig. 13 A, with input variables of the reference state the two apical fluxes, J_V^{tm} and J_V^g, reverse at an external hyperosmolality of ∼30 and 55 mM, respectively. Fig. 13 B depicts the dependence of the net flux of water on luminal osmolarity ($J_V^{net} = J_V^g + J_V^{tm} = J_V^s + J_V^{bm}$). The computations showed that, $J_V^{net} =$ 0.000 nl·cm^{-2}·s^{-1}, if the concentration of the non-diffusible osmolyte was increased to, $\hat{C}_{ND}^o = 31.487$ mM. Thus, $J_V^g + J_V^{tm} = J_V^s + J_V^{bm} \cong 0$ for an external osmotic concentration of, $C_S^g + \hat{C}_{ND}^o = 331.487$ mM. Following Weinstein and Stephenson (1981), this is a measure of the

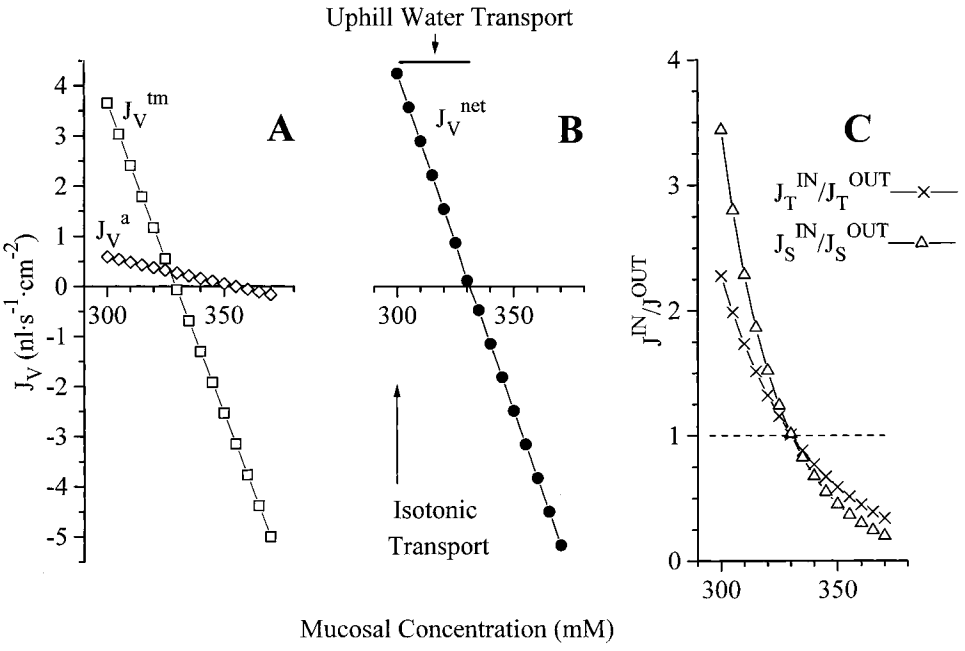

Figure 13. Uphill water transport. (A) With water channels of all five membranes (Table I) both transcellular and paracellular water transport may take place against an adverse osmotic gradient, here accomplished by adding a non-diffusible osmolyte (*ND*, C^o_{ND}) to mucosal bath with $C^o_S = C^i_S = 300$. The driving force is depending on the concentration of the driving solute in *lis* (see text for detailed discussion). The slope of the two relationships depends on the water permeability of the translateral (J^a_V) and the transjunctional (J^{tm}_V) pathway, respectively. (B) The net flux reverses for, $J^a_V + J^{tm}_V = 0$. In its reference state the model accomplishes uphill water transport in the range 0 mM $< C^o_{ND} + 300 <$ ~331 mM. *C*: For diffusible solutes sharing same population of convection-diffusion channels with, $P^{tm}_T/P^{tm}_S = P^{bm}_T/P^{bm}_S = P_T/P_S$, is the ratio of paracellular fluxes of the model given by Eq. 35 in the text. In the example shown is P_T/P_S = 1.5 corresponding to the ratio of the diffusion coefficients in water of Cs^+ and Na^+.

strength of transport. With $\sigma^{bm} \approx 0$, and in experiments conducted with $C^o_S = C^i_S = C^{bath}_S$, and $p^o = p^i = p^{bath}$, it follows (Eqs. 9–10, 12, and 13) that $J^{net}_V = 0$ is fulfilled for:

$$\hat{C}^o_{ND} = \frac{L^{tm}\sigma^{tm}(C^{lis}_S - C^{bath}_S)}{L^{tm} + L^a} + \frac{(L^a + L^s)(C^{cell}_S + C^{cell}_{ND} - C^{bath}_S)}{L^{tm} + L^a} + \frac{(L^{tm} + L^{bm})(p^{bath} - p^{lis}) + (L^a + L^s)(p^{bath} - p^{cell})}{RT(L^{tm} + L^a)} \quad (33)$$

The strength of transport, therefore, is a function of both paracellular and cellular transport parameters including the hydraulic conductance of the epithelium. If modelling is confined to the paracellular pathway, net volume flow ceases when, $J^{tm}_V = J^{bm}_V = 0$, implying that, $J^{tm}_S = P^{tm}_S(C^{bath}_S - C^{lis}_S)$, $J^{bm}_S = P^{bm}_S(C^{lis}_S - C^{bath}_S)$, and $p^{lis} = p^{bath}$. Thus, with mass conservation of lateral space (Eq. 15), at zero paracellular volume flow Eq. 33 reduces to:

$$\hat{C}^o_{ND} = \frac{\sigma^{tm} J^o_{S\,ump}}{P^{tm}_S + P^{bm}_S} \quad (34)$$

This equation shows, for a lateral intercellular space-model is the strength of transport depending, simply, on the ratio of the active solute flux into the lateral space and the sum of ion permeabilities governing the dissipative solute fluxes out of this space. It is noted that Eq. 34 does not contain the hydraulic conductance of the pathway. These were the conclusions of Weinstein and Stephenson (1981), who arrived at an equation similar to Eq. 34 in their modelling of the lateral space.

For the set of computations shown in Fig. 13, the solute concentration of *lis* at which volume flow just ceases is, $C^{lis}_S = 354.857$ mM with $p^{lis} = 1.00137$ atm. Thus, the driving force for volume flow in tight junction is outward resulting in a water flux of, $J^{tm}_V = -0.250$ nl·s^{-1}·cm^{-2} (Eq. 11) that is numerically equal to the influx of water across the apical membrane. This example illustrates a major result given by modelling both cellular and paracellular pathways for volume and ion flows, that is, intraepithelial water fluxes may prevail despite the transepithelial net water flux is zero. The associated paracellular flux-ratio of the driving solute, *S*, together with the flux-ratio of the paracellular tracer, *T*, are shown in Fig. 13 C. If the two molecules share convection-diffusion pores of the delimiting membranes of *lis* with similar selectivity, i.e., $P^{tm}_T/P^{tm}_S = P^{bm}_T/P^{bm}_S = P_T/P_S$, and with $C^o_S = C^i_S$, $C^o_T = C^i_T$, according to Eq. 32 the relationship between the ratios of paracellular unidirectional fluxes would be:

$$\left(\frac{J^{IN}_S}{J^{OUT}_S}\right) = \left(\frac{J^{IN}_T}{J^{OUT}_T}\right)^{\frac{P_T}{P_S}} \quad (35)$$

which is the result of model computations (Fig. 13 C, $P_T/P_S = 1.5$)[8]. At the external concentration at which

[8]In Nedergaard et al. (1999) Cs^+ was used as a paracellular marker. If tight-junction and interspace basement membrane pores are water filled and the two cations move through these pores with no specific interaction with pore walls, the selectivity would be given by the ratio of their diffusion coefficients in water, $D_{Cs}/D_{Na} \approx 1.5$.

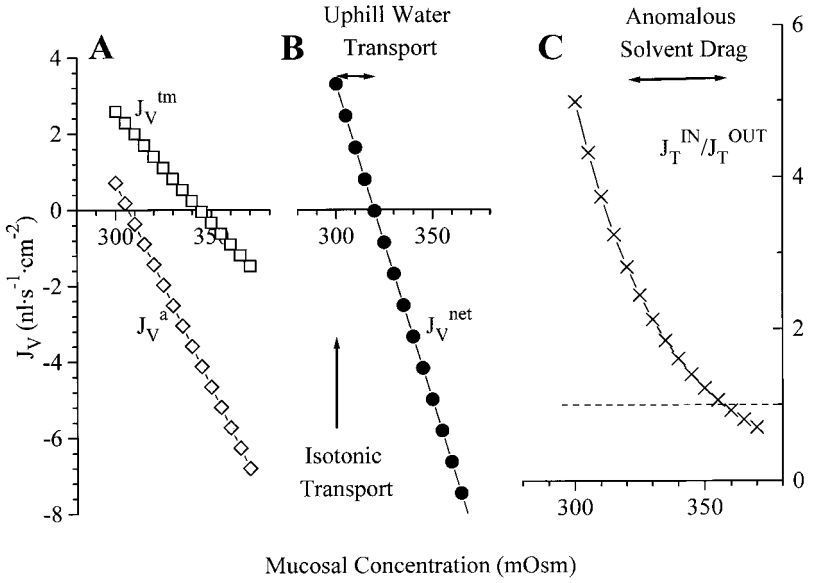

Figure 14. The recirculation model accomplishes uphill water transport and anomalous solvent drag with same choice of membrane-parameter values. This was here achieved by increasing the water permeability of the apical and serosal membranes (by a factor of 10). (A) By adding to the outer bath a non-diffusible solute (*ND*) water is now transported backwards through the cells for $C^o_{ND} > \sim 8$ mM (compare with graphs of FIG. 13 A). (B) By stepwise increase of the concentration of the non-diffusible molecule of the luminal solution from 0 to 70 mM the epithelium is revealing three types of transepithelial water flows: Isotonic water transport, uphill water transport, and net water transport in outward direction with, (C) paracellular solvent drag in inward direction, here illustrated with the ratio of unidirectional fluxes of the paracellular marker molecule, J_T^{IN}/J_T^{OUT}. Reference state values (Table I) except for the following variables: $P_S^{tm} = 3.21\cdot10^{-7}$ cm·s^{-1}, $P_S^{bm} = 5\cdot10^{-6}$ cm·s^{-1}, $P_T^{tm} = 4.82\cdot10^{-7}$ cm·s^{-1}, $P_T^{bm} = 7.5\cdot10^{-6}$ cm·s^{-1}; $\sigma^{tm} = 0.80$; $L^a = 1\cdot10^{-6}$ (cm·s^{-1})·(N·cm^{-2})$^{-1}$, $L^s = 1\cdot10^{-6}$ (cm·s^{-1})·(N·cm^{-2})$^{-1}$.

net water flux is zero, the ratio of the paracellular tracer-flux is less than unity. This follows from the fact mentioned that the condition, $J_V^{net} = 0$, is accomplished with non-zero water flows at the apical and basal boundaries of the epithelium, and that a flux-ratio less than unity is obtained when, $J_V^{tm}(1-\sigma^{tm})/P_S^{tm} + J_V^{bm}(1-\sigma^{bm})/P_S^{bm} < 0$ (Eq. 32, $C_S^o = C_S^i$). In the present computations (Fig. 13) is $J_V^{net} = 0.000$ for $J_V^{tm} = -0.250$, and $J_V^{bm} = 1.017$ nl·cm^{-2}·s^{-1}, respectively, thus $J_S^{para,IN}/J_S^{para,OUT} = 0.95$. The general conclusion is that with circular water flows across the outer and inner boundaries of the epithelium a paracellular flux-ratio less than unity does not necessarily imply that the water flux across both delimiting membranes of the lateral space is outward.

The external concentration at which net water flow reverses (Fig. 13 B) is remarkably different from that observed in studies of rat jejunum (see Discussion). Model analysis of gallbladder by Weinstein and Stephenson (1981) disclosed a similar disagreement between computations and experimental results reported by Whitlock and Wheeler (1964) and Diamond (1964a). Following their theoretical analysis, which took into account paracellular resistance estimates of gallbladder (Reuss and Finn, 1977), we may assume that the paracellular solute permeability is reduced with increased luminal osmolarity. As predicted from Eq. 34 by reducing the permeability of the delimiting membranes better agreements between experiments and computations would be obtained at larger luminal concentrations. For example, with P_S^{tm} and P_S^{bm} decreased by a factor of 7, and with $\sigma^{tm} = 0.80$, the net water flow reverses at an external concentration of 445 mM, i.e., $C^o_{ND} =$ 145 mM (computations not shown). If the paracellular tracer permeabilities are decreased correspondingly, the ratio of paracellular tracer fluxes is 1.41 at a luminal concentration of 450 mM, which compares with a ratio of 1.36 obtained in $^{134}Cs^+$-flux studies of toad small intestine with 150 mM urea added to the luminal perfusion solution (Nedergaard, 1999).

Anomalous solvent drag. Eq. 33 indicates that the hydraulic conductance of the cellular membranes constitutes another membrane variable of significance for the epithelium's capacity for uphill water transport. Also here we will demonstrate the feature by a minimum of changes of the input variables. For maintaining the strength of transport along the paracellular pathway its parameters were kept at the values indicated in the section above (see also legend of Fig. 14), but with the water permeability of the apical and the serosal membrane increased by a factor of 10. Fig. 14, A and B, shows that the high cellular water permeability now results in reversed net water flow already at an external concentration of ~310 mM. However, there is a substantial inward flow of water between cells (Fig. 14 A). This results in a range of external osmolarities in which net water flux is outward, but, nevertheless, the ratio of the paracellular tracer-flux is larger than unity (J_T^{IN}/J_T^{OUT}, Fig. 14 C). Furthermore, by inspection of Fig. 14 it can be seen that there is a range of external osmotic concentrations (345–355 mM) of which the water flux across tight junction is outward, but the flux-ratio of the paracellular marker molecule is above unity. As mentioned above, such a behavior follows from Eq. 32, that is, for luminal concentrations below 355 mM is the argument of this equation positive and the flux ratio >1. The combination of an outward net water flux and a paracellular flux-ratio above unity was first observed in so-called leaky frog skin, and it was denoted

anomalous solvent drag (Ussing, 1966). Since this paper appeared the mechanism has been unknown. The example shown here does not pretend to model frog skin, but to illustrate that anomalous solvent drag in our model is a simple consequence of having parallel flows of water through the epithelium of which the outward cellular flow is driven by transcellular osmosis, and the paracellular inward flow is coupled to active solute transport. Another general conclusion is, with hydraulic conductance of cell membranes the flux of water across cells may obscure the strength of transport of the metabolically driven mechanism.

Pseudo-Solvent Drag

If tight junction water permeability, but not solute permeability, is zero, water enters the lateral space via cells and paracellular markers enter the space via tight junctions. For this limiting case convection occurs in the interspace basement membrane, only. With starting point in our reference state we achieved this in two steps. Firstly, the hydraulic and diffusion permeability of tight junction convection-diffusion pores were decreased by a factor of 10^6 with the diffusion permeability of the pure diffusion channels of tight junction set to, $P_S^{tm,diff} = 1.5{\cdot}10^{-6}$ cm·s^{-1} (driving solute) and $P_T^{tm,diff} = 2.25{\cdot}10^{-6}$ cm·s^{-1} (paracellular marker), respectively, i.e., similar to those of the convection-diffusion pore of the reference state (Table I). Since water now passes the cells of low hydraulic conductance, at steady state the osmotic concentration of the lateral space is significantly increased (to 408 mM) and so is the recirculation flux ($-J_S^g/J_S^{ump} = 0.87$, computations not shown). For obtaining more realistic values of these variables it is necessary to increase the hydraulic conductance of the translateral route. We will illustrate important features of the pseudo-solvent drag mechanism by arbitrarily increasing the values of all three plasma membrane hydraulic conductances (L^a, L^s, and L^{lis}) by a factor of five, which brought C_S^{lis} and $-J_S^g/J_S^{ump}$ closer to the values of the reference state (see Fig. 15). The net solute flux of 756 pmol·s^{-1}·cm^{-2} and the paracellular influx of 433 pmol·s^{-1}·cm^{-2} are within the range of fluxes measured experimentally (Table II). With vanishing small tight junction water permeability and pure diffusion governing tight junction flux of *S*, all sets of mathematical solutions, necessarily $C_S^{lis} > C_S^g$, would be characterized by net diffusion loss of the driving species from *lis* to the outer compartment, in casu, $J_S^{tm} = -47.0$ pmol·s^{-1}·cm^{-2} (Fig. 15). Thus, also across the apical border is there recirculation of the driving species. However, with eliminated tight junction water permeability, and with the above mentioned choice of independent variables, the paracellular flux ratio of the driving species and of paracellular marker are significantly smaller than those estimated experimentally, $J_S^{para,IN}/J_S^{para,OUT} = 1.15$ and $J_T^{para,IN}/J_T^{para,OUT} = 1.10$, respectively.[9] The paracellular flux-ratios can be raised by decreasing the interspace basement membrane solute permeability by a factor of more than five, or by further increasing the hydraulic conductance of serosal membrane such as to obtain an even larger recirculation flux of water across the inner border of the epithelium (computations not shown, but see Eq. 36a). But this adds nothing to the major conclusion, that is, as none of the maneuvers proposed seem justified, it is indicated that with eliminated tight junction water permeability and with physiologically relevant choice of independent variables the model cannot possibly reproduce all aspects of measured cation fluxes in toad small intestine.

With diffusion pores of tight junction and convection-diffusion pores of the interspace basement membrane, according to Eqs. 25a and 25b the paracellular flux-ratio would be independent of the permeability coefficient of tight junction:

$$\frac{J_S^{para,IN}}{J_S^{para,OUT}} = \frac{C_S^g}{C_S^i} \cdot \exp\left(\frac{J_V^{bm} \cdot (1-\sigma^{bm})}{P_S^{bm}}\right) \tag{36a}$$

The relationship between the flux-ratios of two paracellular markers, *S* and *T*, with $C_S^g = C_S^i$ and $C_T^g = C_T^i$, would then be:

$$\left(\frac{J_T^{IN}}{J_T^{OUT}}\right) = \left(\frac{J_S^{IN}}{J_S^{OUT}}\right)^{\frac{P_S^{bm}}{P_T^{bm}}} \tag{36b}$$

Since the reflection coefficient of the interspace basement membrane is small, within a certain range of molecular size we can write, $P_S^{bm}/P_T^{bm} \approx D_S/D_T$, i.e., with little error the exponent of Eq. 36b can be replaced by the ratio of the two molecules' diffusion coefficient in water. This analysis indicates that by proper choice of paracellular marker, a significant paracellular flux-ratio can be generated in an epithelium with water entering the paracellular space via cells, only. In a study of guinea-pig gallbladder, Whittembury et al. (1980) showed that sucrose, inulin, and dextrans of molecular mass of 15,000–17,000 Dalton could be used as paracellular markers exhibiting convective fluxes. We will take the sodium ion and the inulin molecule as examples: $D_{Na} = 1.33{\cdot}10^{-5}$ cm^2·s^{-1} (Robinson and Stokes, 1970); with a molar mass of inulin of 5,000 Dalton, according to the method of Setlow and Pollard (1962), $D_{inulin} \approx 0.2{\cdot}10^{-5}$ cm^2·s^{-1}. Thus, with the paracellular flux-ratio of the driving species being 1.15 (Fig. 15) according to Eq. 36b, that of inulin would be 2.5. While this calcula-

[9] It is not contradictory that the net flux of *S* is directed from *lis* to outer bath (see Fig. 15) while the paracellular flux-ratio of *S* is greater than one. We may here think of the paracellular fluxes as being determined with isotopes different from the isotope pumped into *lis*. Generally, a molecule produced or consumed within a membrane will not influence the ratio of unidirectional tracer fluxes flowing across the membrane (Ussing, 1952).

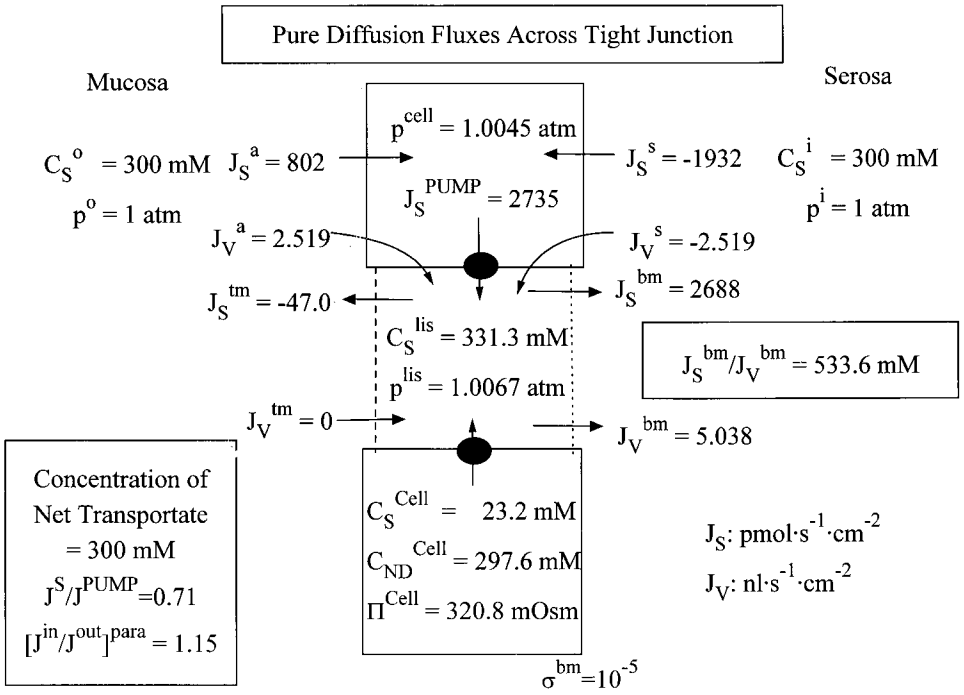

Figure 15. In this version of the model the reference state was modified by eliminating convective flows across tight junction so that *S* and paracellular markers pass this membrane by diffusion, only. Note that the flux of the driving solute is here directed from lateral space to outer compartment, i.e., also across the outer border of the epithelium is there recirculation of the driving solute. Reference-state values (Table I) except for the following variables: P_S^{tm} = 1.5·10^{-12} cm·s^{-1}, $P_S^{tm,diff}$ = 1.5·10^{-6} cm·s^{-1}, P_T^{tm} = 2.25·10^{-12} cm·s^{-1}, $P_T^{tm,diff}$ = 2.25·10^{-6} cm·s^{-1}, L^{tm} = 7.5·10^{-13} (cm·s^{-1})·(N·cm^{-2})$^{-1}$, L^a = 5·10^{-7} (cm·s^{-1})·(N·cm^{-2})$^{-1}$, L^s = 5·10^{-7} (cm·s^{-1})·(N·cm^{-2})$^{-1}$, L^{lm} = 2·10^{-6} (cm·s^{-1})·(N·cm^{-2})$^{-1}$.

tion presupposes that also the second species (here *T* = inulin) can permeate tight junction, the result is independent of the selectivity of tight junction.

DISCUSSION

This study deals with a simple mathematical description and computer assisted analysis of the recirculation theory for solute-coupled water absorption. This type of transport is in the body found in so-called leaky epithelia of, e.g., (reviews) small intestine (Chang and Rao, 1994; Madara and Trier, 1994), gallbladder (Reuss, 1991), kidney proximal tubule (Dantzler, 1992; Weinstein, 1992), and possibly also in upper airways (Boucher, 1994a,b, 1999). The theory belongs to the family of theories that assumes coupling between solute and water flows in an intraepithelial compartment lined with active solute pumps. Unlike previous formulations (e.g., Ogilvie et al. 1963; Diamond and Bossert, 1967; Huss and Marsh, 1975; Sackin and Boulpaep, 1975; Weinstein and Stephenson, 1981; Weinstein, 1986), the recirculation theory assumes that metabolic energy is not only used for generating a hypertonic and hyperbaric intraepithelial space, but also in the subsequent regulation of the tonicity of the transportate. It is further assumed that both works are performed by a common population of solute pumps, that is, in vertebrate epithelia, Na^+/K^+-pumps.

In this first stage of our analysis, the mathematical description is simplified by considering solute transports in an electroneutral regime, so that a non-electrolyte rather than the charged sodium ion constitutes the driving species. The reason why we expect that such a description gives useful insights into some general aspects of the mechanism of solute-coupled fluid transport is that in many leaky epithelia is the transepithelial electric potential difference close to zero. During physiological activity convection-diffusion constitutes the major, in some cases the only, mechanism of transepithelial paracellular flow of diffusible ions. Furthermore, some ion pathways of luminal and serosal cell membranes are co- and counter transporters working in an electro-neutral fashion (for vertebrate small intestine, reviewed by, e.g., Chang and Rao, 1994; Madara and Trier, 1994; see also Nedergaard et al., 1999). Together with published studies, in the following are discussed in more detail six features pertinent to epithelia performing solute-coupled water transport.

Isotonic Fluid Transport in Absence of External Transepithelial Driving Force

With exactly similar solute composition, hydrostatic pressure, and electrical potential, respectively, of the two external compartments, truly isotonic transport occurs when the tonicity of transported fluid is identical with the tonicity of bathing solutions. Previous models dealing with coupling in a well-stirred intraepithelial compartment of solute and water fluxes, account for near-isotonic transport, only. That is to say, extracellular solution's tonicities are identical within experimental error of measurements, which is ~2%. Thus, in one type of modelling (Weinstein and Stephenson, 1981) it is accepted that the outside solution is slightly hypotonic or, vice versa, that the inner solution is slightly hypertonic. The strategy of the analysis, then, is to iden-

tify conditions where the transportate's tonicity is identical with one of the bathing solutions. Accordingly, one has skipped the requirement that the system operates at truly transepithelial thermodynamic equilibrium. Other types of modelling (Sackin and Boulpaep, 1975) assume identical bathing solutions and accept that tonicity of the transportate becomes hypertonic. Here the requirement of an isotonic transportate is abandoned. In both types of modelling are the conditions for near-isotonic transport limited to particular sets of values of independent variables rendering acceptable mathematical solutions confined by narrow boundary conditions.

Cation fluxes of small intestine (Nedergaard et al., 1999) provide reference data for the present model, which has resulted in computed recirculation fluxes in agreement with experimental analysis (Table II). In the computations we assumed a non-constant solute permeability of serosal membrane, which returns the solute to the pump, and solved the set of equations with requirement that the ratio of net solute flux and net water flux is equal to the tonicity of external bathing solutions (in casu, 300 mM). In contrast with the above mentioned previous theoretical analyses, our modelling results in truly isotonic transport with many combinations of solute and water permeabilities of cell and interspace membranes. Analyses showed that this was achieved with the (virtual) tonicity of the fluid emerging from the lateral intercellular space spanning a large range and, thus, with different demands on recirculation (Figs. 5, 8, 10, 11, 12, and 15). Notably, under all conditions was it checked that the tonicity of the lateral intercellular fluid was compatible with physiological situations, and that the paracellular flux-ratio was within range of measured values. Thus, the recirculation model exhibits a high degree of flexibility for precisely adjusting the performance when large perturbations are imposed on its membrane properties. This fundamentally novel feature is due to, (a) in a convection-diffusion regime, at steady state the tonicity of the fluid emerging from the lateral space does not reflect the tonicity of the lateral intercellular fluid (Figs. 2, 3, and 15), and (b) recirculation releases the demand that composition of the fluid exiting the lateral space would have to be within a narrow range about isotonicity. In order for this mechanism to work, the epithelium must possess two parallel pathways, (a) a pathway allowing for modest hydrostatic pressure build-up and convective flow, and (b) a recirculation pathway, allowing for recirculation of the solute without convective flow. In different versions of the model we assumed that the *lis* constitutes the first pathway, but with water being drawn through both the tight junctions and the cell, or only through the cell. In both cases, the basal membrane of the cell constitutes the recirculation pathway. Thus we have followed the suggestion of Whitlock and Wheeler (1964) and Diamond and Bossert (1967) that the *lis* constitutes the coupling compartment between water and solute, but in agreement with Diamond and Bossert (1967) and Boulpaep et al. (1993) we point out that other structures may be involved, such as the basal infoldings of the renal proximal tubule. The basic novel feature of the recirculation model is a differentiation in function between the part of the basolateral membrane facing the coupling compartment (*lis*, infoldings), and the rest of the basolateral membrane. This postulated differentiation constitutes the major testable assumption of the model. The recirculation pathway of the serosal membrane could be a Na^+-K^+-$2Cl^-$-cotransporter (discussed in Nedergaard et al., 1999), but this is unknown. It is an explicit assumption that the activity of epithelial transporters (quite likely, but not necessarily P_S^s, see Computing Strategy) is being regulated according to demand of recirculation. This is emphasized in Fig. 10, where recirculation flux is increased/maintained with increasing cellular concentration of the driving solute, something that could not be achieved without regulation.

With tonicity of the transported fluid set to that of the external compartments (Eq. 27) it follows that the model generates isotonic transport whatever external osmolality is assumed (Table III). This remarkable feature was demonstrated for rabbit gallbladder by Diamond (1964a,b), who varied the ambient osmolality over a range of eightfold. With no further assumptions the model predicts (Table III) the hitherto unexplained decreased efficiency of active sodium transport in gallbladder exposed to diluted bathing solutions (Frederiksen and Leyssac, 1969). While the efficiency was decreased by more than 50% in gallbladder the computed decrease is $\sim$20% in response to reduction of external osmolality from 300 to 150 mM. Computed results presented in Table III also show that the observed activation of fluid absorption upon bilateral dilution of the external bathing solutions (Diamond, 1964b; Frederiksen and Leyssac, 1969) is not being reproduced. The tentative conclusion is that regulatory mechanisms not included in the model are operating in the biological preparation.

Our analysis addresses the debated question about the driving force for water movement from mucosal solution to lateral space. In a study with ion sensitive microelectrodes of electrolyte concentrations of the lateral intercellular space fluid Ikonomov et al. (1985) concluded that the transjunctional osmotic gradient in *Necturus* gallbladder is no more than 1–2 mosmol$\cdot l^{-1}$. From an electro-physiological study of *Ambystoma* proximal tubule Sackin (1986) concluded that the interspace [NaCl] is $\sim$4% above that of bathing solutions, and he suggested that this space normally can function as coupling compartment for transepithelial salt and

water reabsorption under bilateral isotonic conditions. By loading the *lis* of MDCK cells with the fluorescent dye, SBFQ, Chatton and Spring (1995) found that the *lis* Na^+-concentration was 15 mM above that of the bathing solutions. The in situ calibration applied involved comparison to periods where ouabain blocked pump fluxes. This means that the increased Na^+-concentration was due to pump activity. Notably, Chatton and Spring (1995) found no gradient along the *lis*, in agreement with our compartmental model.

Our computations indicate similar small gradients and predict that even large water flows can be associated with small osmotic concentration difference between mucosal and interspace solutions without compromising the robustness of the system (p. 14; Fig. 12; and Table III).

Transport of Water Uphill

Our model contains two pathways for transepithelial water movement, the paracellular pathway and the cellular pathway. Water flows between cells and from cells to *lis* are driven by the pump, while water flow through cells is driven by the transepithelial osmotic gradient imposed by the investigator. Thus, the transepithelial osmotic gradient at which net uphill water movement stops is given by the balance between the pump-driven water influx and the water permeability of the cell membranes. With an adverse osmotic gradient across the epithelium, if the pump-driven water flux is larger than the backward flux of water through cells, the epithelium exhibits uphill transport of water (Fig. 13). Parsons and Wingate (1958) showed that rat jejunum is capable of absorbing water from a luminal solution made hypertonic by varying its NaCl concentration. The flux of water decreased with increasing luminal osmotic concentration, and was still significant with the (initial) lumen concentration being 130 mM above that of the (initial) serosal bath. Nedergaard (1999) applied $^{134}Cs^+$ as paracellular marker in experiments with toad small intestine. With 100 mM urea, or 100 mM mannitol, added to mucosal bath, the $^{134}Cs^+$ flux-ratio was still significantly above unity, indicating inward convective fluxes of $^{134}Cs^+$, and thus paracellular flow of water against an adverse transepithelial osmotic gradient. These two sets observations were reproduced by decreasing the paracellular solute permeability (p. 17). Agreements within a larger range of external osmolarities between experiments and model computations would be possible, e.g., by assuming that the paracellular permeability is a continuous of function of the external concentration. However, due to lack of experimental measurements further model adjustments would be arbitrary and add nothing to our conclusion, i.e., the Weinstein-Stephenson-equation (see Eq. 34) is of major significance also in our model. Finally, we can conclude (Eq. 33; Figs. 13 and 14) that in models with paracellular and cellular pathways for ion and water transport, the capacity for uphill water transport is also depending on the magnitude of the transcellular water permeability.

Paracellular Convection Fluxes

In leaky epithelia, hydrophilic solutes entering the lateral intercellular space via tight junction exhibit net inward fluxes in the absence of external electrochemical driving forces. It is a generally accepted hypothesis that this is accomplished by a transepithelial flow of water that entrains the solutes (Frömter et al., 1973; Hill and Hill, 1978; Andreoli et al., 1979; Whittembury et al., 1980, 1988). Paracellular convection fluxes were demonstrated in two qualitatively different configurations of the model. The first one is configured with water channels in tight junction and convection-diffusion fluxes in both tight junction and interspace basement membrane. In this configuration conventional solvent drag can be analyzed. In the other configuration, tight junction hydraulic conductance was eliminated so that water enters the lateral space via cells through lateral water channels, whereas paracellular markers enter this space by diffusion through water impermeable channels of tight junction, which results in pseudo-solvent drag. Pseudo-solvent drag has been associated with unstirred layers (reviewed in Barry and Diamond, 1984), but our analysis has shown that the phenomenon is more general, being associated also with translateral fluid flow in well-stirred compartments. In this configuration the driving species is also recirculated across the apical border of the epithelium (Fig. 15). Kovbasnjuk et al. (1995) applied fluorescence microscopy to the lateral space between MDCK cells loaded with a fluorescent Na^+-sensitive probe, and measured apical and basal Na^+ permeabilities of the lateral pathway. It was shown, during absorption Na^+ leaks out via tight junctions indicating that it would be recirculated. Using confocal laser microscopy Kovbasnjuk et al. (1998) extended the above study by estimating convection induced concentration profiles in the lateral intercellular space of the slowly diffusing fluorescin dextran. They arrived at the conclusion that the water flux is zero at the level of tight junctions. The computations above lead to the conclusion that in epithelia configured like the MDCK cells, under transepithelial thermodynamic equilibrium conditions lateral pumps would drive convective fluxes of paracellular markers in the inward direction. For the compartment model of Fig. 1 our treatment has shown that paracellular flux-ratios are given by Eqs. 36a and 36b.

Anomalous Solvent Drag

Anomalous solvent drag refers to the paradox that epithelia generating osmotic water flux in outward direc-

tion may exhibit inwardly directed net flux of paracellular marker molecules maintained at transepithelial thermodynamic equilibrium (Ussing, 1966; Franz and Van Bruggen, 1967). Our model accomplishes this type of transport, and predicts that it is also driven by lateral solute pumps. Anomalous solvent drag was analyzed with convection-diffusion fluxes across tight junction. It is a simple consequence of having water flowing both via paracellular and cellular pathways. It is an interesting feature of the recirculation model that isotonic transport, uphill water transport, and anomalous solvent drag can all be simulated with the same set of membrane parameters (Fig. 14). To our knowledge the recirculation model constitutes the first theoretical description, which can deal with isotonic transport and anomalous solvent drag within a common framework.

Large Isotonic Fluid Flows Associated With High Density of Sodium Pumps

Our computations reproduced Curran's (1960) finding that the transepithelial water uptake depends on transepithelial active Na^+ transport, and that these two fluxes vary in proportion with one another (Fig. 10 A). Similar to previous models (Weinstein and Stephenson, 1981), also in the recirculation model is the density of pumps on lateral membranes governing the maximal rate of fluid transport across the epithelium (Fig. 12). This is in agreement with experimental findings indicating that those epithelia exhibiting the largest flow of water, like mammalian proximal tubule, also have the largest density of sodium pumps. With a relatively small apical solute permeability the entrance to the cells is rate limiting for volume flow (Fig. 11), because the driving solute passes the cellular pool. In an experimental study of rabbit gallbladder Spring and Hope (1979) found that the rate of exchange of the intracellular NaCl pool (after external osmotic perturbations) is of a magnitude similar to the active transepithelial flux of the salt under control conditions. They concluded that apically absorbed Na^+ (and Cl^-) passes the cell pool before being pumped into the lateral space. In the recirculation model this is so whether water flow is predominantly transjunctional (Fig. 3) or exclusively translateral (Fig. 15).

Energetic Cost of Active Sodium Transport Spans Large Range

In tight epithelia like frog skin and vertebrate urinary bladder the sodium pump transports ~18 Na^+ per molecule O_2 consumed (Zerahn, 1956; Leaf and Renshaw, 1957; Leaf and Dempsey, 1960). This number is compatible with a stoichiometry of the pump of 3 Na^+ transported per ATP hydrolyzed. This is contrasting the leaky frog skin, which transports five to six times less sodium ions per molecule of oxygen consumed (Ussing, 1966). As discussed above, the cost of sodium transport in rabbit gallbladder also varies with experimental conditions. By replacing Ringer's solutions with solutions of about half Ringer's strength the efficiency decreased from 30.4 to 13.5 mol Na^+/mol O_2. It was suggested that a pump other than the sodium pump drives solutes and water through the leaky epithelium (Frederiksen and Leyssac, 1969). A high energetic efficiency of Na^+ transport was indicated also in the first study of gallbladder (24.6 mol Na^+/mol O_2, Martin and Diamond, 1966). Similar high values of efficiencies have been measured in experiments with mammalian kidney (25–30 mol Na^+/mol O_2; Deetjen and Kramer, 1961; Lassen and Thaysen, 1961; Lassen et al., 1961; Thurau, 1961; Torrelli et al., 1966).

Our computations show that recirculation of the driving solute through cells may result in metabolic energy expenditure that is significantly larger than would be predicted from the net active transport (Fig. 3; Table III). Our analysis also revealed conditions at which recirculation is small and paracellular convection-diffusion relatively large so that net absorption of the driving solute would occur with an overall efficiency larger than that of the pump itself (Fig. 12; Table III). Thus, the recirculation model accounts in a simple way for the above-mentioned paradoxical findings.

The study was supported by the Danish Natural Science Research Council (11-0971).

Submitted: 14 May 1999
Revised: 31 May 2000
Accepted: 1 June 2000

REFERENCES

Andreoli, T.E., and J.A. Schafer, S.L. Troutman, and M.L. Watkins. 1979. Solvent drag component of Cl^- flux in superficial proximal straight tubules: evidence for a paracellular component of isotonic fluid absorption. *Am. J. Physiol.* 237:F455–F462.

Atisook, K., S. Carlson, and J.L. Madara. 1990. Effects of phlorizin and sodium on glucose-elicited alterations of cell junctions in intestinal epithelia. *Am. J. Physiol.* 258:C77–C85.

Barry, P.H., and J.M. Diamond. 1984. Effects of unstirred layers on membrane phenomena. *Physiol. Rev.* 64:763–872.

Benzel, C.J, M. Davies, W.N. Scott, M. Zatsman, and A.K. Solomon. 1968. Osmotic volume flow in the proximal tubule of *Necturus* kidney. *J. Gen. Physiol.* 51:517–533.

Boucher, R.C. 1994a. Human airway ion transport. Part One. *Am. J. Respir. Crit. Care. Med.* 150:271–281.

Boucher, R.C. 1994b. Human airway ion transport. Part Two. *Am. J. Respir. Crit. Care. Med.* 150:581–593.

Boucher, R.C. 1999. Molecular insights into the physiology of the thin film of airway surface liquid. *J. Physiol.* (*London*) 516:631–638.

Boulpaep, E.L., A.B. Maunsbach, S. Tripathi, and M.R. Weber. 1993. Mechanism of isosmotic water transport in leaky epithelia: consensus and inconsistencies. *In* Isotonic Transport in Leaky Epithelia. *Proc. Alfred Benzon Symp.* Vol. 34. H.H. Ussing, J. Fischbarg, O. Sten-Knudsen, E.H. Larsen, N.J. Willumsen, editors. Munksgaard, Copenhagen. 53–67.

Chang, E.B., and M.C. Rao. 1994. Intestinal water and electrolyte

transport: mechanisms of physiological and adaptive responses. *In* Physiology of the Gastrointestinal Tract. 3rd edition, Vol. 2. D.H. Alpers, Johnson, L, J. Christensen, M. Jackson, E.D. Jacobson, and J. Walsh, editors. Raven, New York. 2027–2081.

Chatton, J.-Y., and K.R. Spring. 1995. The sodium concentration of the lateral intercellular spaces of MDCK cells: A microspectrofluorimetric study. *J. Membrane Biol.* 144:11–19.

Curran, P.F. 1960. Na, Cl, and water transport by rat ileum *in vitro*. *J. Gen. Physiol.* 43:1137–1148.

Curran, P., and J.R. MacIntosh. 1962. A model system for biological water transport. *Nature.* 193:347–348.

Curran, P.F., and A.K. Solomon. 1957. Ion and water fluxes in the ileum of rats. *J. Gen. Physiol.* 41:143–168.

Dantzler, W.H. 1992. Comparative aspects of renal function. *In* The Kidney: Physiology and Pathophysiology: 2nd edition. D.E.W. Seedling, and G. Giebisch, editors. Raven Press, New York. 885–942.

Deetjen, P., and K. Kramer. 1961. Die Abhängigkeit des O_2-Verbrauchs der Niere von der Na-Rückresorption. *Pflügers Arch.* 273: 636–642.

Diamond, J.M. 1964a. Transport of salt and water in rabbit and guinea pig gall bladder. *J. Gen. Physiol.* 48:1–14.

Diamond, J.M. 1964b. The mechanism of isotonic water transport. *J. Gen. Physiol.* 48:15–42.

Diamond, J.M., and W.H. Bossert. 1967. Standing-gradient osmotic flow. A mechanism for coupling of water and solute transport in epithelia. *J. Gen. Physiol.* 50:2061–2083.

Franz, T.J., and J.T. Van Bruggen. 1967. Hyperosmolarity and the net transport of non-electrolytes in frog skin. *J. Gen. Physiol.* 50: 933–949.

Frederiksen, O., and P. Leyssac. 1969. Transcellular transport of isosmotic volumes by the rabbit gall-bladder. *J. Physiol.* 210:201–224.

Frizzell, R.A., and S.G. Schultz. 1972. Ionic conductances of extracellular shunt pathway in rabbit ileum. Influence of shunt on transmural sodium transport and electrical potential differences. *J. Gen. Physiol.* 59:318–346.

Frömter, E., G. Rumrich, and K.J. Ullrich. 1973. Phenomenologic description of Na^+, Cl^- and HCO_3^- absorption. *Pflügers Arch.* 343:189–220.

Hénin, S., D. Cremaschi, T. Schettino, G. Meyer, C.L.L. Donin, and F. Cotelli. 1977. Electrical parameters in gallbladders of different species. Their contribution to the origin of the transmural potential difference. *J. Membr. Biol.* 34:73–91.

Hertz, G. 1922. Ein neues Verfahren zur Trennung von Gasgemischen durch Diffusion. *Physik. Z.* 23:433–434.

Hill, A.E., and B.S. Hill. 1978. Sucrose fluxes and junctional water flow across *Necturus* gall bladder epithelium. *Proc. R. Soc. Lond. B Biol. Sci.* 200:163–174.

Huss, R.E., and D.J. Marsh. 1975. A model of NaCl and water flow through paracellular pathways of renal proximal tubule. *J. Membrane Biol.* 23:305–347.

Ikonomov, O., M. Simon, and E. Frömter. 1985. Electrophysiological studies on lateral intercellular space in *Necturus* gallbladder epithelium. *Pflügers Arch.* 403:301–397.

Kedem O., and A. Katchalsky. 1958. Thermodynamic analysis of the permeability of biological membranes to non-electrolytes. *Biochim. Biophys. Acta.* 27:229–246.

Kovbasnjuk, O., J.-Y. Chatton, W.S. Friauf, and K.R. Spring. 1995. Determination of the Na permeability of the tight junctions of MDCK cells by fluorescence microscopy. *J. Membr. Biol.* 148:223–232.

Kovbasnjuk, O., J.P. Leader, A.M. Weinstein, and K.R. Spring. 1998. Water does not flow across the tight junctions of MDCK cell epithelium. *Proc. Natl. Acad. Sci. USA.* 95:6526–6530.

Larsen, E.H., and J.N. Sørensen. 1999. A mathematical model of fluid transporting leaky epithelia incorporating recirculation of the driving solute. *FASEB J.* 13:A74–A111.7.

Lassen, U.V., and J.H. Thaysen. 1961. Correlation between sodium transport and oxygen consumption in isolated renal tissue. *Biophys. Biochem. Acta.* 47:616–618.

Lassen, N.A., O. Munk, and J.H. Thaysen. 1961. Oxygen consumption and sodium reabsorption in the kidney. *Acta Physiol. Scand.* 51:371–384.

Leaf, A., and E. Dempsey. 1960. Some effects of mammalian neurohypophyseal hormones on metabolism and active transport of sodium by the isolated toad bladder. *J. Biol. Chem.* 235:2160.

Leaf, A., and A. Renshaw. 1957. Ion transport and respiration of isolated frog skin. *Biochem. J.* 65:82.

Madara, J.L., and J.S. Trier. 1994. The functional morphology of the mucosa of the small intestine. *In* Physiology of the Gastrointestinal Tract. 3rd edition, Vol. 2. D.H. Alpers, L. Johnson, J. Christensen, M. Jackson, E.D. Jacobson, and J. Walsh. Raven, editors. New York. 1577–1622

Martin, D.W., and J.M. Diamond. 1966. Energetics of coupled active transport of sodium and chloride. *J. Gen. Physiol.* 50:295–315.

Nedergaard, S. 1999. Sodium recirculation and isotonic water transport across isolated toad intestine. *Physiol. Res.* 48(Suppl.): S100.

Nedergaard, S., E.H. Larsen, and H.H. Ussing. 1999. Sodium recirculation and isotonic transport in toad small intestine. *J. Membr. Biol.* 168:241–251.

Ogilvie, J.T., J.R. McIntosh, and P.F. Curran. 1963. Volume flow in a series-membrane system. *Biochim. Biophys. Acta.* 66:441–444.

Parsons, D.S., and D.L. Wingate. 1958. Fluid movement across wall of rat small intestine *in vitro*. *Biochem. Biophys. Acta.* 30:666–667.

Patlak, C.S., D.A. Goldstein, and J.F. Hoffman. 1963. The flow of solute and solvent across a two-membrane system. *J. Theoret. Biol.* 5:426–442.

Reuss, L.A. 1991. Salt and water transport by gallbladder epithelium. *In* Handbook of Physiology. Sect 6, Vol. IV. American Physiological Society, Washington, DC. 303–322.

Reuss, L., and A.L. Finn. 1977. Effects of luminal hyperosmolality on electrical pathways of *Necturus* gallbladder. *Am. J. Physiol.* 232: C99–C108.

Robinson, R.A., and R.H. Stokes. 1970. Electrolyte Solutions, 2nd edition. Butterworths, London, 571 pp.

Sackin, H. 1986. Electrophysiology of salamander proximal tubule. II: interspace NaCl concentration and solute coupled water transport. *Am. J. Physiol.* 251:F334–F347.

Sackin, H., and E.M. Boulpaep. 1975. Models for coupling of salt and water transport. *Proximal tubular reabsorption in Necturus kidney. J. Gen. Physiol.* 66:671–733.

Schafer, J.A., S.L. Troutman, M.L. Watkins, and T.E. Andreoli. 1978. Volume absorption in the pars recta. I. "Simple" active Na^+ transport. *Am. J. Physiol.* 234:F332–F339.

Setlow, R.B., and E.C. Pollard. 1962. Molecular Biophysics. Addison-Wesley Publishing Company, Inc., Reading, MA. 545 pp.

Smoluchowski, M.V. 1915. Ueber Brownsche Molekularbewegung unter Einwirken äuserer Kräfte und deren Zusammenhang mit der verallgemeinerten Diffusionsgleichung. *Ann. Physik.* 48: 1103–1112.

Spring, K.R., and A. Hope. 1979. Fluid transport and dimensions of cells and interspace of living *Necturus* gallbladder. *J. Gen. Physiol.* 73:287–305.

Sten-Knudsen, O. 1978. Passive transport processes. *In* Membrane Transport in Biology. Vol. I. Concepts and Models. G. Giebisch, D.C. Tosteson, H.H. Ussing, editors. Springer-Verlag, New York. 5–113.

Thurau, K. 1961. Renal Na-reabsorption and O_2 uptake in dogs

during hypoxia and hydrochlorothiazide infusion. *Proc. Soc. Exp. Biol. Med.* 106:714–717.

Torrelli, G.E., E. Milla, A. Faelli, and S. Costantini. 1966. Energy requirement for sodium reabsorption in the in vivo rabbit kidney. *Am. J. Physiol.* 211:576–580.

Ussing, H.H. 1952. Some aspects of the application of tracers in permeability studies. *Adv. Enzymol.* XIII:21–65.

Ussing, H.H. 1966. Anomalous transport of electrolytes and sucrose through the isolated frog skin induced by hypertonicity of the outside bathing solution. *Annu. NY Acad. Sci.* 137:543–555.

Ussing, H.H., and K. Eskesen. 1989. Mechanism of isotonic water transport in glands. *Acta Physiol. Scand.* 136:443–454.

Ussing, H.H, and S. Nedergaard. 1993. Recycling of electrolytes in small intestine of toad. *In* Isotonic Transport in Leaky Epithelia. Vol. 34. H.H. Ussing, J. Fischbarg, O. Sten-Knudsen, E.H. Larsen, and N.J. Willumsen, editors. *Proc. Alfred Benzon Symp.* Munksgaard, Copenhagen. 25–34

Ussing H.H., and K. Zerahn. 1951. Active transport of sodium as the source of electric current in the short-circuited isolated frog skin. *Acta Physiol. Scand.* 23:110–127.

Ussing, H.H., F. Lind, and E.H. Larsen. 1996. Ion secretion and isotonic transport in frog skin glands. *J. Membr. Biol.* 152:101–110.

Weinstein, A.M. 1986. A mathematical model of rat proximal tubule. *Am. J. Physiol.* 254:F297–F305.

Weinstein, A.M. 1992. Sodium and chloride transport. *In* The Kidney. Physiology and Pathophysiology. 2nd edition, Vol 2. D.W. Seldin, and G. Giebisch, editors. Raven Press, New York. 1925–1973.

Weinstein, A.M. 1994. Mathematical models of tubular transport. *Annu Rev. Physiol.* 56:691–709.

Weinstein, A., and J.L. Stephenson. 1981. Models of coupled salt and water transport across leaky epithelia. *J. Membr. Biol.* 60:1–20.

Welling, L.W., and J.J. Grantham 1972. Physical properties of isolated perfused renal tubules and tubular basement membrane. *J. Clin. Invest.* 51:1063–1075.

Whitlock, R.T., and Wheeler, H.O. 1964. Coupled transport of solute and water across rabbit gallbladder epithelium. *J. Clin. Invest.* 43:2249–2265.

Whittembury, G., and L. Reuss. 1992. Mechanism of coupling of solute and solvent transport in epithelia. *In* The Kidney. Physiology and Pathophysiology. 2nd edition, Vol 1. D.W. Seldin and G. Giebisch, editors. Raven Press, New York. 317– 360.

Whittembury, G., C.V. De Martínez, H. Linares, and A. Paz-Aliaga. 1980. Solvent drag of large solutes indicates paracellular water flow in leaky epithelia. *Proc. R. Soc. Lond. B.* 211:63–81.

Whittembury, G, G. Malnic, M. Mello-Aires, and C. Amorena. 1988. Solvent drag of sucrose during absorption indicates paracellular water flow in the rat kidney proximal tubule. *Pflügers Arch.* 412: 541–547.

Windhager, E.E., G. Whittembury, D.E. Oken, H.J. Schatzmann, and A.K. Solomon. 1958. Single proximal tubules of the Necturus kidney. III. Dependence of H_2O movement on NaCl concentration. *Am. J. Physiol.* 197:313–318.

Worman, H.J., and M. Field. 1985. Osmotic water permeability of small intestine brush-border membranes. *J. Membr. Biol.* 87:233–239.

Zerahn, K. 1956. Oxygen consumption and active sodium transport in the isolated and short-circuited frog skin. *Acta Physiol Scand.* 36:300–318.